Horikawa et al. Progress in Earth and Planetary Science (2015) 2:19
DOI 10.1186/s40645-015-0048-3

Progress in Earth and Planetary Science
a SpringerOpen Journal

RESEARCH ARTICLE Open Access

$\delta^{18}O_{sw}$ estimate for *Globigerinoides ruber* from core-top sediments in the East China Sea

Keiji Horikawa[1*], Tomohiro Kodaira[2], Jing Zhang[1] and Masafumi Murayama[3]

Abstract

The paired analyses of the Mg/Ca ratio and oxygen isotopic composition ($\delta^{18}O_c$) of surface-dwelling planktonic foraminifera have become a widely used method for reconstructing the oxygen isotopic composition of ambient seawater ($\delta^{18}O_{sw}$) as a robust proxy for surface salinity. *Globigerinoides ruber* (*G. ruber*) is a mixed-layer dweller, and its fossil shell is an ideal archive for recording past sea surface water conditions, such as those caused by variability in the East Asian summer monsoon (EASM). Here, we investigate the validity of shell-derived $\delta^{18}O_{sw}$ estimates for *G. ruber* using core-top sediments from the East China Sea (ECS). First, we determined a local $\delta^{18}O_{sw}$–salinity equation for the eastern part of the ECS in July [$\delta^{18}O_{sw} = -7.74 + 0.23 \times salinity$]. Then, we calculated $\delta^{18}O_{sw}$ from core-top $\delta^{18}O_c$ and Mg/Ca values in *G. ruber* using the $\delta^{18}O_c$–temperature equation of Bemis et al. (Paleoceanography 13(2):150–160, 1998) and the Mg/Ca–temperature equation of Hastings et al. (EOS 82:PP12B-10, 2001). The core-top $\delta^{18}O_{sw}$ and salinity were estimated to be in the ranges of −0.2 to +0.39 ‰ and 33.7 to 34.5, respectively, which fall close to the local $\delta^{18}O_{sw}$–salinity regression line. The core-top data showed that the Mg/Ca–temperature calibration by Hastings et al. (EOS 82:PP12B-10, 2001) and the $\delta^{18}O_c$–temperature equation by Bemis et al. (Paleoceanography 13(2):150–160, 1998) are appropriate for calculating $\delta^{18}O_{sw}$ in the ECS. Furthermore, we measured core-top Ba/Ca ratios of *G. ruber* ($Ba/Ca_{G.\ ruber}$), which ranged from 0.66 to 2.82 μmol mol^{-1}. There was not a significant relationship between the salinity and $Ba/Ca_{G.\ ruber}$ ratios due to the highly variable $Ba/Ca_{G.\ ruber}$ data. Given the seawater Ba/Ca data and the published partition coefficient for Ba ($D_{Ba} = 0.15–0.22$), pristine $Ba/Ca_{G.\ ruber}$ ratios at northern Okinawa Trough sites should be less than 0.84 μmol mol^{-1}. Anomalously high $Ba/Ca_{G.\ ruber}$ ratios (>0.84 μmol mol^{-1}) might be attributable to contamination by sedimentary barite adherent on fossil shells. Therefore, further evaluation of the $Ba/Ca_{G.\ ruber}$ ratio as a paleo-salinity proxy requires diethylene triamine pentaacetic acid (DTPA)-cleaned Ba/Ca data that can minimize the influence of barite contamination.

Keywords: Oxygen isotope composition of seawater; Reconstruction of sea surface salinity; Mg/Ca–temperature; *Globigerinoides ruber*; East China Sea

Background

An East Asian summer monsoon (EASM) precipitation zone is formed by the convergence of a westerly flow to the north of the Tibetan Plateau and a southerly monsoon flow over eastern China, which gradually moves northward from South China and reaches northern China in late July (Qian and Lee 2000). This EASM precipitation has caused anomalous climatic events (both wet and dry) on an inter-decadal scale, influencing the agricultural production and economy in Asia (Wang 2006). Paleoclimate records show that anomalous dry periods, when summer monsoons weakened, caused crop failure and led to the collapse of some Chinese dynasties (Yancheva et al. 2007). Therefore, EASM variability, its effect on remote areas, and the mechanisms behind this variability have been investigated intensively as important climate change issues (Wang et al. 2005; Chen et al. 2008; Wang et al. 2008; Chang et al. 2009; Liu et al. 2014).

The EASM brings a large amount of precipitation to South China and the drainage area of the Changjiang River (Yangtze River) and induces a large influx of Changjiang River runoff to the East China Sea (ECS), forming Changjiang diluted water (CDW) in the

* Correspondence: horikawa@sci.u-toyama.ac.jp
[1]Graduate School of Science and Engineering for Research, University of Toyama, Gofuku 3190, Toyama 930-8555, Japan
Full list of author information is available at the end of the article

Changjiang River Estuary (Zhang et al. 1990; Chen et al. 1994) (Fig. 1). The CDW extends farther offshore, driven by the southerly and southwesterly monsoons from June to August, and advection of the CDW causes a significant decrease in the sea surface salinity (SSS) of the northern Okinawa Trough (Chang and Isobe 2003; Lee and Chao 2003). Consequently, the northern Okinawa Trough is considered an oceanic area where EASM-related variability in SSS can be seen (Chang and Isobe 2003).

In such areas, the oxygen isotopic compositions of seawater ($\delta^{18}O_{sw}$) have been estimated from paired analyses

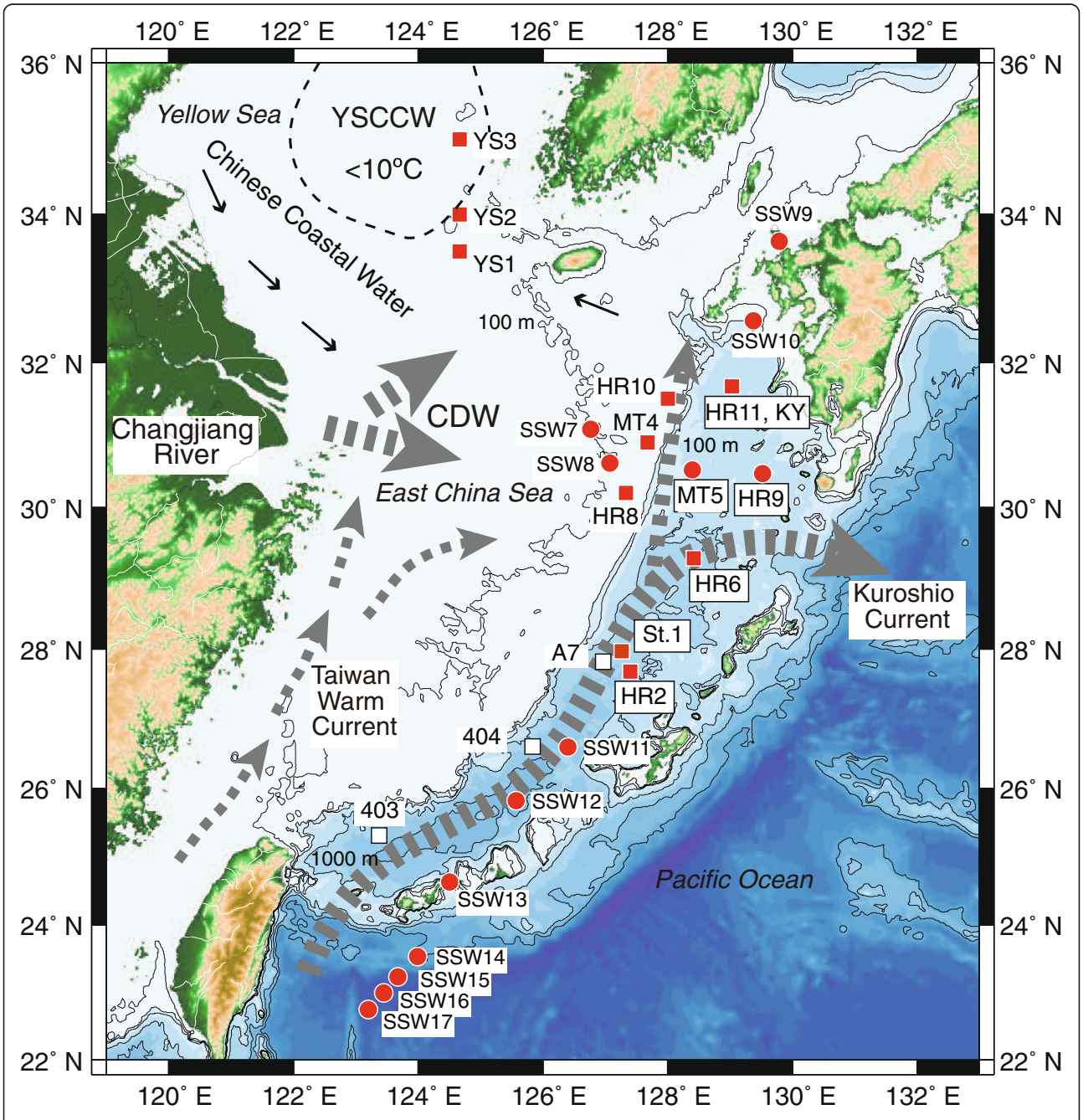

Fig. 1 Map of sample locations. Locations for surface seawater samples (*red circles*) and surface–subsurface seawater samples (*red squares*) are shown together with the present current system (Ichikawa and Beardsley 2002). Surface sediments were taken from HR11, MT5, HR9, HR6, HR2, and St.1. Locations for sediment core at KY, A7, 403, and 404 (Sun et al. 2005; Lin et al. 2006; Chen et al. 2010; Kubota et al. 2010) are also shown. CDW and YSCCW represent the Changjiang diluted water and Yellow Sea Central Cold Water, respectively. The bathymetric contours represent 100, 200, 300, 1000, 2000, and 3000 m

of Mg/Ca temperatures and oxygen isotopes ($\delta^{18}O_c$) in the surface-dwelling foraminifera *Globigerinoides ruber* (*G. ruber*) to reconstruct EASM-related variability in SSS (Sun et al. 2005; Kubota et al. 2010). However, $\delta^{18}O_{sw}$ estimates from paired analyses of Mg/Ca temperatures and $\delta^{18}O_c$ in planktonic foraminifera entail high levels of uncertainty (>0.2 ‰) due to the propagation error of $\delta^{18}O_c$ and Mg/Ca measurements and Mg/Ca–temperature calibration (Schmidt 1999; Rohling 2007). Furthermore, the lack of a local $\delta^{18}O_{sw}$–salinity equation causes additional uncertainties in salinity estimates calculated from $\delta^{18}O_{sw}$ values. Additionally, if the habitat of *G. ruber* shifts seasonally, independent of EASM variability, shell-derived $\delta^{18}O_{sw}$ estimates also change, and interpreting EASM variability will be complicated. Therefore, a reliable reconstruction of SSS with respect to EASM variability requires adequate Mg/Ca–temperature, $\delta^{18}O_c$–temperature, and local $\delta^{18}O_{sw}$–salinity calibration equations and an understanding of the habitat season and depth of *G. ruber* in the ECS.

In this study, we first derive a local $\delta^{18}O_{sw}$–salinity equation for the northern Okinawa Trough to provide a basis for salinity estimates calculated from $\delta^{18}O_{sw}$ for *G. ruber*. Then, using ECS core-top sediments, we calculate the core-top $\delta^{18}O_{sw}$ from Mg/Ca ratios and $\delta^{18}O_c$ for *G. ruber* and compare them with the local $\delta^{18}O_{sw}$–salinity line. We find that the Mg/Ca–temperature calibration by Hastings et al. (2001) and the $\delta^{18}O_c$–temperature equation by Bemis et al. (1998) are appropriate for calculating $\delta^{18}O_{sw}$ in the ECS. Finally, we present the Ba/Ca ratios of *G. ruber* from ECS core-top sediments for the first time and discuss the possibility of using shell Ba/Ca ratios as an independent paleo-salinity proxy in the ECS.

Oceanographic setting

The ECS is a marginal sea in the northwestern Pacific bounded by China, Taiwan, Ryukyu Island, Kyushu, and the Korean Peninsula (Fig. 1). The Yellow Sea is located in the northern part of the ECS, with most (>70 %) of both the Yellow Sea and ECS located above the continental shelf (<200 m water depth). The deep Okinawa Trough (~2000 m water depth) is a back-arc basin that occupies the remaining southeastern part of the ECS (Ichikawa and Beardsley 2002).

The Yellow Sea and the ECS receive the saline and warm Kuroshio water that enters the ECS along the east of Taiwan and flows northeastward along the shelf slope in the ECS (Fig. 1). The annual cycle of Kuroshio volume transport has an estimated maximum of 24 Sv (1 Sv = 1×10^6 m^3 s^{-1}) in the summer and a minimum of 20 Sv in the autumn (Lee et al. 2001). In addition, the Taiwan warm current (TWWC), which originates from the Kuroshio, flows into the ECS from the South China Sea (SCS) through the Taiwan Strait off western Taiwan, with an annual mean northward transport of 0.78 Sv (Jan et al. 2006; Zhang et al. 2014) (Fig. 1). In the autumn and winter, Changjiang River runoff decreases (1.0×10^4 m^3 s^{-1} in January) (Yanagi 1994), and the CDW flows southwestward along the Chinese coast as a narrow band; the saline water (>34) of Kuroshio origin enters the Yellow Sea (Chang and Isobe 2003). However, during the summer, when the Changjiang River supplies a large amount of freshwater to the ECS (4.8×10^4 m^3 s^{-1} in July) (Yanagi 1994), the CDW starts to extend offshore and spread east- and northeastward. Then, the eastward-flowing CDW mixes with the TWWC and the Kuroshio water in the southern and eastern parts of the ECS, respectively (Chang and Isobe 2003) (Fig. 2a).

Since the annually averaged precipitation and evaporation are near equilibrium in the ECS and Yellow Sea and the Changjiang River runoff accounts for 90 % of the total river discharge (with an annual mean of ~3.0×10^4 m^3 s^{-1}), the Changjiang River discharge is considered the dominant freshwater source in the ECS (Beardsley et al. 1985; Chen et al. 1994; Yanagi 1994). This Changjiang River water extends offshore, and therefore, the water mass characteristics of the offshore ECS can be roughly described by the binary mixing of the cooler, less saline CDW and the warmer, more saline Kuroshio water (Zhang et al. 1990; Ichikawa and Beardsley 2002; Zhang et al. 2007). In contrast, there are other local water masses in the coastal ECS and the Yellow Sea, such as the TWWC and the Yellow Sea Central Cold Water (YSCCW) (Fig. 1). Therefore, the water mass characteristics and $\delta^{18}O_{sw}$–salinity relationships of the coastal ECS are more complicated than those of the offshore ECS, as discussed in a later section.

The northern Okinawa Trough, which is the main focus of this study, shows distinct seasonal changes in SSS (e.g., site HR11, SSS = 33.2–34.7) due to the advection of the CDW, in comparison with the central Okinawa Trough (e.g., site HR2, SSS = 34.4–34.8) (Figs. 1 and 2a). Sea surface temperature (SST) distribution also varies seasonally owing to monsoonal winds (Lee and Chao 2003). The climatological mean annual SST is 22.2 °C near site HR11 in the northern Okinawa Trough, with a maximum in August (28.1 °C) and a minimum in February (17.5 °C). In the central Okinawa Trough, the mean annual SST is 25.0 °C near site HR2, with a maximum in August (28.9 °C) and a minimum in February (21.5 °C) (Japan Oceanographic Data Center (JODC), available at http://www.jodc.go.jp/).

Methods

Seawater and sediment samples

Seawater samples were collected using a CTD (conductivity, temperature, and depth) Carousel multisampling

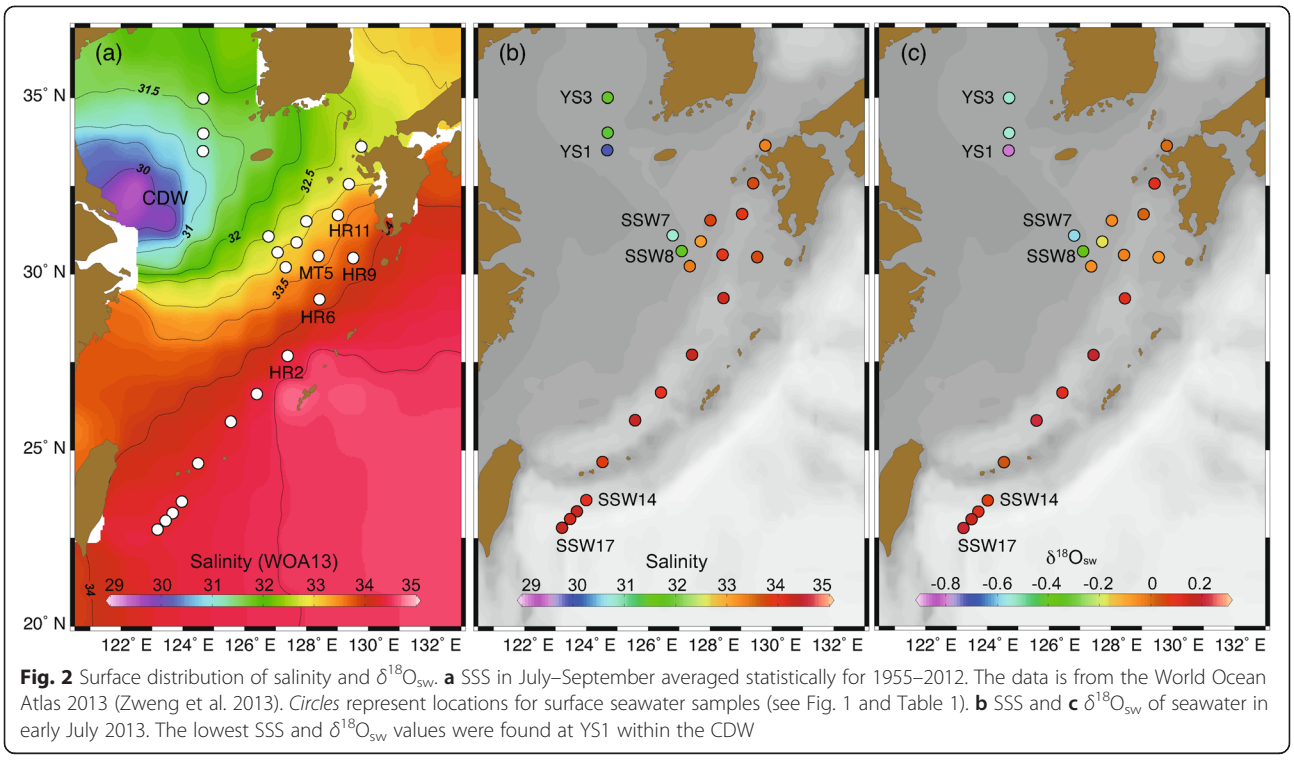

Fig. 2 Surface distribution of salinity and $\delta^{18}O_{sw}$. **a** SSS in July–September averaged statistically for 1955–2012. The data is from the World Ocean Atlas 2013 (Zweng et al. 2013). *Circles* represent locations for surface seawater samples (see Fig. 1 and Table 1). **b** SSS and **c** $\delta^{18}O_{sw}$ of seawater in early July 2013. The lowest SSS and $\delta^{18}O_{sw}$ values were found at YS1 within the CDW

system (Sea-Bird, model SBE 9plus) during the KH-13-4 cruise in early July 2013 (R/V Hakuho Maru) (Table 1). The CTD system has 24 attached Niskin bottles, each with a volume of 12 L. Subsurface seawater samples were taken with the Niskin bottles, and surface water samples were taken using a bucket (~0 m depth) or pumped from below the ship (~5 m depth). All seawater samples were transferred into glass vials for salinity and $\delta^{18}O_{sw}$ measurements, and the samples for the $\delta^{18}O_{sw}$ measurements were stored at 4 °C until laboratory analysis. Salinity was measured with an onboard Autosal laboratory salinometer (Model 8400B, Guildline Instruments Ltd., Canada) and is reported using the practical salinity scale. Sampling vials for salinity were prepared according to Joint Global Ocean Flux Study (JGOFS) protocols. The Autosal was standardized using International Association for the Physical Sciences of the Oceans (IAPSO) standard seawater.

Three sampling stations (YS1–3) are located in the southwest area off the Korean Peninsula, and 19 other stations (MT, HR, and SSW sites) are located in the continental shelf slope area of the ECS and in the Pacific Ocean (Fig. 1). We report salinity and $\delta^{18}O_{sw}$ data from these stations, and the vertical profiles of both datasets were obtained for nine stations (Fig. 1 and Table 1). Surface sediment samples were taken by a multiple corer at six sites along the central to northern parts of the Okinawa Trough from water depths of 709 to 1675 m during the KH-13-4 and KT-12-25 cruises (Fig. 1 and Table 2). Sediment samples were subsampled onboard with a 1 cm resolution and stored in a refrigerator until analysis in the laboratory.

The lithology of the sediment cores (~30 cm core length) was characterized as foraminifer-bearing silty clay or clayey silt with no visible turbidities or erosional surfaces. In general, the central to northern parts of the Okinawa Trough preserve thick late Holocene sediments due to their high sedimentation rates (10–50 cm kyr^{-1}), except in shelf slope regions (Ujiié et al. 2003; Sun et al. 2005; Kubota et al. 2010). All core-top $\delta^{18}O_c$ values of *G. ruber* were isotopically lighter than −2.0 ‰, which is consistent with the late Holocene values in the central to northern Okinawa Trough (Table 2) (Sun et al. 2005; Kubota et al. 2010). Therefore, we conclude that the core-top sediments used in this study represent at least late Holocene sediments. Site HR2 was located at a depth below the present calcite saturation horizon (CSH) in the ECS (~1600 m) (Fig. 6a). The Mg/Ca ratios from this site should be treated with caution regarding the partial dissolution of *G. ruber* shells, which will be discussed in a later section.

Analysis of the oxygen isotopic composition of seawater ($\delta^{18}O_{sw}$)

We measured $\delta^{18}O_{sw}$ with a stable isotope mass spectrometer (PRISM, Micromass UK, Ltd.) at the University of Toyama. Oxygen isotopic analysis was carried out using the automated H_2O–CO_2 equilibrium method

Table 1 Salinity and $\delta^{18}O_{sw}$ data at each station in the ECS

Depth (m)	Temperature (°C)	Salinity	$\delta^{18}O_{sw}$ (‰, VSMOW)	Std.dev (‰)	Site area
YS1 (30 June 2013, 124° 39.66′ E, 33° 29.80′ N)					Yellow Sea–ECS shelf site
0	23.40	29.89	−0.81	0.03	
5	22.95	30.60	−0.67	0.03	
10	22.83	31.51	−0.47	0.02	
20	17.10	32.82	−0.18	0.02	
40	10.17	33.05	−0.12	0.02	
YS2 (30 June 2013, 124° 40.07′ E, 34° 00.40′ N)					Yellow Sea–ECS shelf site
0	22.90	31.37	−0.54	0.03	
5	22.80	31.50	−0.52	0.02	
10	22.76	31.86	−0.43	0.03	
20	17.14	32.35	−0.35	0.04	
30	13.54	32.57	−0.29	0.03	
YS3 (1 July 2013, 124° 40.04′ E, 34° 59.64′ N)					Yellow Sea–ECS shelf site
0	23.90	31.88	−0.53	0.03	
5	23.12	31.86	−0.52	0.03	
10	17.29	31.87	−0.48	0.02	
20	13.73	32.09	−0.44	0.02	
30	7.71	32.21	−0.42	0.02	
HR8 (2 July 2013, 127° 19.84′ E, 30° 12.68′ N)					Yellow Sea–ECS shelf site
0	26.70	33.40	−0.06	0.02	
20	25.50	33.90	0.07	0.02	
40	24.09	34.34	0.15	0.02	
60	21.33	34.58	0.27	0.02	
70	19.44	34.61	0.26	0.02	
MT4 (2 July 2013, 127° 41.25′ E, 30° 54.42′ N)					Yellow Sea–ECS shelf site
0	26.10	33.10	−0.18	0.02	
6	25.81	33.16	−0.19	0.02	
10	25.79	33.37	−0.14	0.04	
30	24.44	33.81	0.00	0.03	
60	21.56	34.19	0.10	0.02	
100	19.08	34.64	0.20	0.02	
HR10 (2 July 2013, 128° 00.21′ E, 31° 30.22′ N)					Yellow Sea–ECS shelf site
0	26.10	33.75	−0.04	0.02	
5	25.87	33.68	−0.08	0.02	
10	25.80	33.82	−0.02	0.02	
20	25.49	34.07	0.05	0.02	
40	24.96	34.20	0.09	0.02	
59	22.91	34.39	0.17	0.04	
80	21.01	34.59	0.22	0.02	
99	19.86	34.65	0.24	0.03	
HR11 (2 July 2013, 129° 01.85′ E, 31° 40.60′ N)					Okinawa Trough site
0	26.90	33.88	0.01	0.02	
49	23.76	34.30	0.15	0.02	

Table 1 Salinity and $\delta^{18}O_{sw}$ data at each station in the ECS *(Continued)*

75	21.96	34.56	0.23	0.02	
99	20.27	34.69	0.24	0.04	
HR6 (8 July 2013, 128° 25.43′ E, 29° 17.42′ N)					Okinawa Trough site
0	29.70	34.22	0.12	0.05	
20	29.57	34.23	0.11	0.02	
50	28.63	34.35	0.23	0.02	
75	27.21	34.52	0.27	0.04	
99	23.69	34.66	0.33	0.04	
HR2 (9 July 2013, 127° 24.03′ E, 27° 40.97′ N)					Okinawa Trough site
0	29.40	34.25	0.18	0.02	
5	29.63	34.24	0.13	0.02	
10	29.36	34.19	0.14	0.03	
20	29.01	34.17	0.14	0.02	
50	26.32	34.40	0.24	0.02	
75	23.86	34.61	0.32	0.02	
100	22.47	34.74	0.35	0.02	
HR9 (7 July 2013, 129° 31.29′ E, 30° 28.26′ N)					Okinawa Trough site
0	28.50	33.73	−0.07	0.03	
MT5 (8 July 2013, 128° 23.41′ E, 30° 31.22′ N)					Okinawa Trough site
0	28.50	33.91	−0.03	0.02	
SSW07 (2 July 2013, 126° 45.99′ E, 31° 04.86′ N)					Yellow Sea–ECS shelf site
5	23.20	30.80	−0.59	0.04	
SSW08 (2 July 2013, 127° 04.33′ E, 30° 37.06′ N)					Yellow Sea–ECS shelf site
5	25.30	31.80	−0.36	0.02	
SSW09 (7 July 2013, 129° 47.01′ E, 33° 38.63′ N)					Off-Kyushu site
5	24.10	33.33	0.00	0.02	
SSW10 (7 July 2013, 129° 22.50′ E, 32° 34.00′ N)					Off-Kyushu site
5	23.60	33.71	0.12	0.05	
SSW11 (9 July 2013, 126° 24.20′ E, 26° 36.00′ N)					Okinawa Trough site
5	28.80	34.00	0.12	0.02	
SSW12 (9 July 2013, 125° 33.84′ E, 25° 49.26′ N)					Okinawa Trough site
5	29.20	34.38	0.21	0.03	
SSW13 (9 July 2013, 124° 30.06′ E, 24° 38.41′ N)					Okinawa Trough site
5	28.80	33.81	0.03	0.02	
SSW14 (10 July 2013, 123° 59.02′ E, 23° 32.27′ N)					Kuroshio site
5	29.30	34.06	0.06	0.02	
SSW15 (10 July 2013, 123° 40.09′ E, 23° 14.07′ N)					Kuroshio site
5	29.30	34.33	0.12	0.09	
SSW16 (10 July 2013, 123° 26.97′ E, 22° 59.89′ N)					Kuroshio site
5	29.40	34.23	0.15	0.02	
SSW17 (10 July 2013, 123° 11.60′ E, 22° 45.00′ N)					Kuroshio site
5	29.40	34.34	0.20	0.02	

Table 2 Details of the core-top sediments and metal/Ca and $\delta^{18}O$ values from *Globigerinoides ruber* (sensu stricto)

Core site	Latitude	Longitude	Water depth (m)	$\delta^{18}O$ (VPDB ‰)		Mg/Ca (mmol mol^{-1})	±SD	Ba/Ca (μmol mol^{-1})	±SD	Mn/Ca (μmol mol^{-1})	±SD
KH13-4-HR2MC	27° 40.79′ N	127° 23.95′ E	1675	−2.93	Ave	4.09	0.18	0.72	0.74	7.88	5.5
					Run #1	4.05		0.66		0.74	
					Run #2	3.94		0.78		6.50	
					Run #3	4.03		1.53		11.58	
					Run #4	4.35		2.25		12.71	
KT12-25-St.1	27° 58′ N	127° 16′ E	1153	−2.52	Ave.	4.20	0.03	0.77	0.01	23.25	21.3
					Run #1	4.22		0.78		8.18	
					Run #2	4.18		0.77		38.31	
KH13-4-HR6MC	29° 17.35′ N	128° 25.18′ E	1065	−2.47	Ave.	3.97	0.25	0.79	0.20	4.37	4.4
					Run #1	3.68		1.04		1.92	
					Run #2	4.13		0.66		9.49	
					Run #3	4.09		0.92		1.72	
KH13-4-HR9MC	30° 28.19′ N	129° 31.06′ E	709	−2.78	Ave.	4.19	0.25	0.81	1.09	53.01	13.7
					Run #1	3.91		0.81		48.40	
					Run #2	4.36		1.11		68.44	
					Run #3	4.30		2.82		42.18	
KH13-4-MT5MC	30° 31.23′ N	128° 23.38′ E	823	−2.27	Ave.	3.61	0.22	0.88	0.11	44.50	7.7
					Run #1	3.41		0.72		51.73	
					Run #2	3.44		0.95		46.37	
					Run #3	3.68		0.97		46.21	
					Run #4	3.89		0.87		33.67	
KH13-4-HR11MC	31° 40.57′ N	129° 01.99′ E	725	−2.42	Ave.	3.30	0.02	0.85	0.06	44.86	37.0
					Run #1	3.31		0.89		18.67	
					Run #2	3.29		0.80		71.05	
A7	27° 49.2′ N	126° 58.7′ E	1264	−2.35		4.06					
MD012403	25° 17′ N	123° 10′ E	1420	−2.51		4.40					
MD012404	26° 38.84′ N	125° 48.75′ E	1397	−2.60		4.24					
KY07-04-01	31° 38.35′ N	128° 56.64′ E	725	−2.50		3.50					

Table 2 Details of the core-top sediments and metal/Ca and $\delta^{18}O$ values from *Globigerinoides ruber* (sensu stricto)

No dissolution-corrected Mg/Ca-derived SST			Dissolution-corrected Mg/Ca-derived SST							
SST[a] (°C)	SST[b] (°C)	SST[c] (°C)	SST[a] (°C)	$\Delta[CO_3^{2-}]$ (μmol kg^{-1})	Corrected Mg/Ca (mmol mol^{-1})	Calcification SST	Shell-derived $\delta^{18}O_{sw}$ (VSMOW ‰)	Calcification salinity	Calcification season	Calcification depth (m)
26.7	24.4	29.4	28.7	−2.3	4.90	28.5	0.22	34.43	July–Sept	0–10
27.0	24.6	29.7	28.0	5.9	4.60	26.6	0.27	34.50	May–Oct	0–30
26.4	24.1	29.0	27.3	7.3	4.30	26.3	0.19	34.41	May–Oct	0–30
27.0	24.6	29.6	27.1	12.9	4.24	27.3	0.01	34.01	June–Sept	0–30
25.3	23.2	27.9	25.7	11.1	3.75	25.1	0.17	34.17	May–Oct	0–30
24.3	22.3	26.9	24.5	12.7	3.37	25.3	−0.20	33.76	June–Sept	0–30
26.6	24.3	29.3	27.9	4.2	4.55	25.9	0.37	34.54	May–Oct	0–30
27.5	25.1	30.2	29.0	1.7	5.01	26.5	0.39	34.43	May and Oct	0–30
27.1	24.7	29.8	28.6	2.1	4.84	26.9	0.21	34.38	May–Oct	0–30
24.9	22.9	27.6	25.2	12.7	3.57	25.6	−0.14	33.68	June–Sept	0–20

Decreases in Mg/Ca ratios due to calcite dissolution were calculated using critical thresholds for the dissolution (14 μmol kg^{-1} $\Delta[CO_3^{2-}]$) and sensitivity of Mg/Ca ratio to $\Delta[CO_3^{2-}]$ (0.05 mmol mol^{-1} per μmol^{-1} kg^{-1}) (Johnstone et al. 2011). Core-top Mg/Ca and $\delta^{18}O$ data from A7, MD012403, MD012404, KY07-04-01 were from Sun et al. (2005), Lin et al. (2006), Chen et al. (2010), and Kubota et al. (2010), respectively

[a]SST = ln(Mg/Ca/0.38)/0.089, Hastings et al. (2001)

[b]SST = ln(Mg/Ca/0.34)/0.102, Anand et al. (2003)

[c]SST = ln(Mg/Ca/0.3)/0.089, Lea et al. (2000)

(Epstein and Mayeda 1953). The stable isotope ratios are given as conventional δ values (‰), and the analytical precision was ±0.02 ‰ (1σ) for $\delta^{18}O$. Oxygen isotopic composition is expressed relative to Vienna Standard Mean Ocean Water (VSMOW).

$\delta^{18}O$ and Mg/Ca analyses of *G. ruber*

Core-top sediments (0–1 cm) were wet washed through a 63 μm sieve and then dried in an oven at 50 °C. To minimize ontogenic and growth rate effects on shell geochemistry, specimens of *G. ruber* (sensu stricto form; 20–30 shells) were handpicked from the 250–355 μm size fraction. Planktonic foraminifera were gently crushed and rinsed three times with ultrapure water and methanol (super special grade, Wako Pure Chemical Industries, Ltd.) to remove adherent clay particles. The shells were then split into two fractions for $\delta^{18}O_c$ and metal/Ca measurements. $\delta^{18}O_c$ values were obtained using a Finnigan MAT 253 mass spectrometer at the Center for Advanced Marine Core Research (CMCR), Kochi University and calibrated in accordance with standard NBS 19. The precision of these measurements was better than ±0.08 ‰ (1σ) for $\delta^{18}O_c$.

The samples for metal/Ca analysis were cleaned according to the procedure developed for trace element analysis (Boyle and Keigwin 1985; Rosenthal et al. 1997). In brief, samples underwent a multistep process consisting of initial rinses in ultrapure water and methanol, followed by treatments with hot reducing and oxidizing solutions, transferred into new acid-leached microcentrifuge tubes (1.5 mL), and finally leached with a dilute ultrapure nitric acid solution (0.001 M HNO_3, TAMAPURE-AA-100 from Tama Chemicals, Ltd.). The sample solution was then dissolved with a Sc-spiked

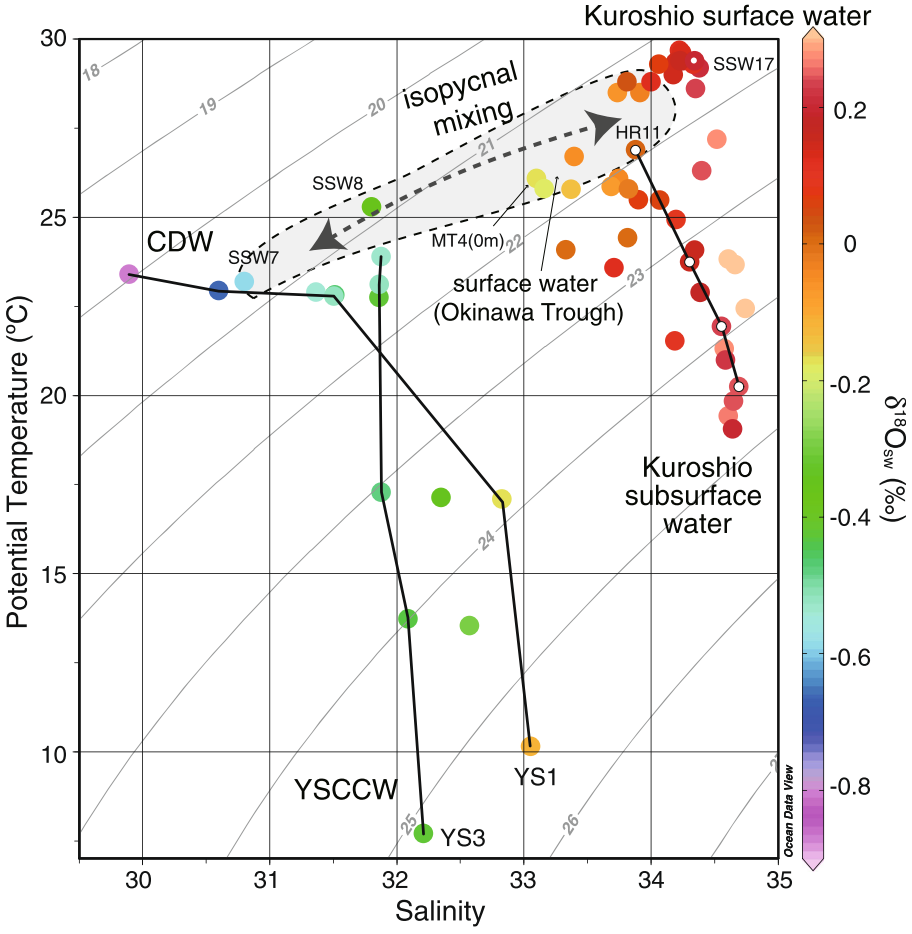

Fig. 3 Potential temperature and salinity (*T–S*) plot in the ECS. The *T–S* diagram shows four distinct water masses in early July: the Kuroshio surface water, Kuroshio subsurface water, YSCCW, and CDW. The *color in circles* indicates the $\delta^{18}O_{sw}$ value of the seawater. The Kuroshio surface and subsurface waters are characterized by higher $\delta^{18}O_{sw}$ values, whereas the CDW is characterized by relatively low $\delta^{18}O_{sw}$ values. Surface water properties in the northern part of the Okinawa Trough can be explained by isopycnal mixing with the CDW and Kuroshio surface water. The potential density curves (σ_θ = 19–27) are also shown. The *T–S* diagram was made using Ocean Data View (Schlitzer R, Ocean Data View, http://odv.awi.de, 2014)

dilute ultrapure nitric acid solution (2 % HNO_3) to obtain a Ca concentration of 10 ± 1 μg g^{-1}. All clean work was conducted in laminar flow benches or a clean room under trace metal clean conditions.

The metal/Ca ratio was determined with a Thermo Scientific ELEMENT 2 sector field inductively coupled plasma mass spectrometer (ICP–MS) at the University of Toyama, operated in a low-resolution mode ($m/\Delta m$ = 300) (Marchitto 2006). We analyzed ^{24}Mg, ^{26}Mg, ^{43}Ca, ^{44}Ca, ^{88}Sr, ^{137}Ba, and ^{138}Ba during the same run to determine Mg/Ca for temperature reconstructions and measured ^{56}Fe (in a mid-resolution mode) and ^{55}Mn to monitor contamination by clay minerals and diagenetic coatings (Table 2). Element counts were converted into molar ratios by the intensity ratio method based on a series of matrix-matched standard solutions. The accuracy and precision of Mg/Ca ratios were confirmed by analyses of the $CaCO_3$ reference materials BAM RS3 and ECRM 752-1. The repeated analyses gave Mg/Ca ratios of 0.786 ± 0.008 (n = 100, 1σ, RSD = 1.0 %) and 3.92 ± 0.06 (n = 24, 1σ, RSD = 1.5 %), respectively, which were within the reported value for BAM RS3 (0.791 ± 0.03) and slightly higher than the reported value for ECRM 752-1 (3.824 ± 0.095) (Greaves et al. 2008). Samples often show high Mn/Ca ratios (>100 μmol mol^{-1}) due to the presence of diagenetic coatings that were not removed during the cleaning process. Such samples were rejected. To further minimize the impact of sample heterogeneity and the analytical error of metal/Ca ratios, we report replicate measurements of metal/Ca ratios on re-picked *G. ruber* shells (Table 2).

Results and discussion

$\delta^{18}O_{sw}$–salinity relationship in the eastern ECS

In early July, surface water samples showed the highest SSS (34.3) at site SSW17 in the Kuroshio water area and the lowest SSS (29.9) at YS1 in the Yellow Sea (Fig. 2b and Table 1). The $\delta^{18}O_{sw}$ ranged from −0.81 to 0.21 ‰, and relatively low $\delta^{18}O_{sw}$ values were observed in the Yellow Sea, the ECS shelf, and the northern part of the Okinawa Trough (Fig. 2c). Spatial distributions of salinity and $\delta^{18}O_{sw}$ values were almost similar to the summer (July–September) salinity distribution averaged statistically over 1955–2012 (Zweng et al. 2013) (Fig. 2a), suggesting that the CDW spread east- and northeastward in the southern Yellow Sea and the northern Okinawa Trough during the sampling period.

A temperature and salinity plot (T–S diagram) of the surface and subsurface waters (0–100 m) in the Yellow Sea and the ECS shows four typical water masses: (1) the Kuroshio surface water in the subtropical Pacific Ocean (e.g., SSW14–17), (2) the Kuroshio subsurface

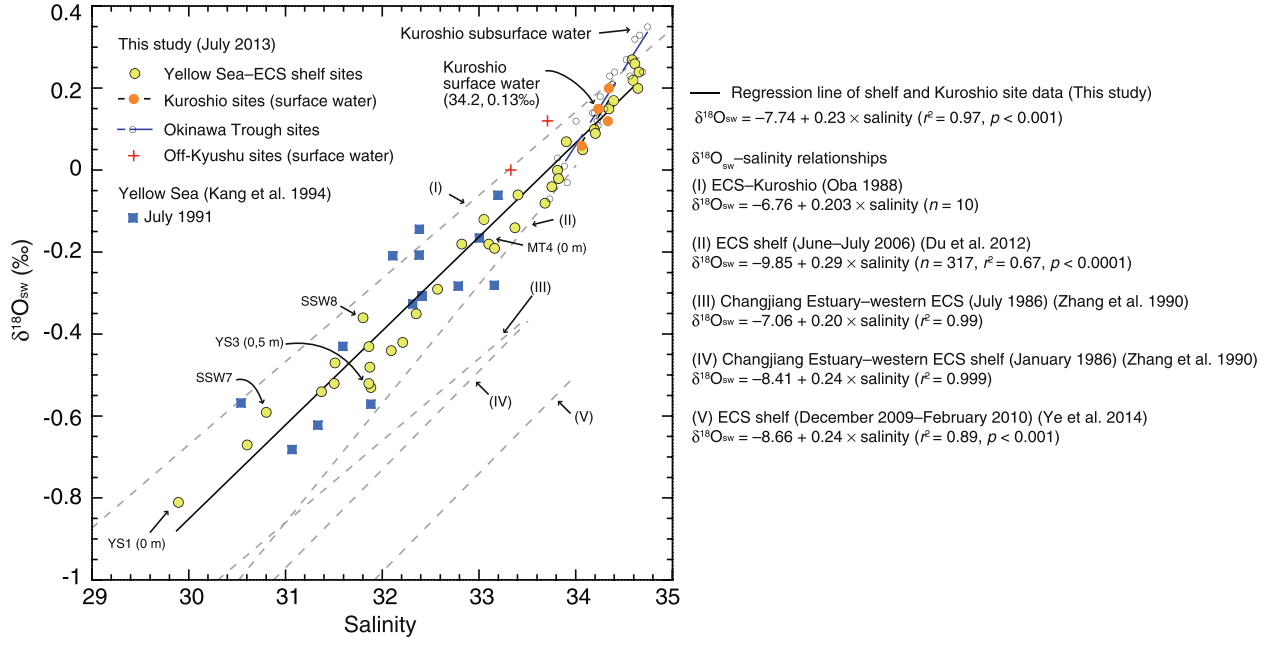

Fig. 4 $\delta^{18}O_{sw}$–salinity plot of shallow seawaters in the ECS. $\delta^{18}O_{sw}$–salinity plot of all shallow seawater (0–100 m) data in this study (early July 2013). The data are classified into four site groups: Yellow Sea–ECS shelf, Kuroshio, Okinawa Trough, and off-Kyushu sites (Table 1). The *black* regression line is derived from the data in the Yellow Sea–ECS shelf and Kuroshio sites. Since the surface waters in the northern Okinawa Trough are a mixture of the CDW and Kuroshio surface water, $\delta^{18}O_{sw}$ and salinity data from northern Okinawa Trough sites fall on this regression line. Regression lines (*dotted lines*) and equations from the literature are also shown. Regression lines III, IV, and V were developed in mainly coastal and shelf waters near the Changjiang Estuary. Although these regression lines represent freshwater end-members that are similar to our regression line, the end-member of the seawater shows lower $\delta^{18}O_{sw}$ values than that of the Kuroshio surface water (34.2 and 0.13 ‰; SSW14–17)

water in the Okinawa Trough (identified by a salinity of ~34.4 and a $\delta^{18}O_{sw}$ of 0.2–0.5 ‰) (Kang et al. 1994; Kim et al. 2005), (3) the YSCCW (<10 °C) in the bottom water (30 m) at YS3, and (4) the less saline CDW in the surface water at YS1 (Fig. 3). The *T*–*S* diagram also shows that the majority of the shallow water data in the Okinawa Trough fall on the isopycnal mixing line connecting the CDW and Kuroshio surface water (Fig. 3). Indeed, the $\delta^{18}O_{sw}$ values and salinity of the shallow seawater (0–100 m) are strongly correlated, indicating that the data can be explained by a binary mixing of freshwater and saline seawater (Fig. 4).

To derive a local $\delta^{18}O_{sw}$–salinity relationship around the northern Okinawa Trough, sampling sites were classified by geographic and oceanographic characteristics (Table 1). Sites SSW14–17, which are outside the ECS and under the influence of the Kuroshio surface water, were defined as Kuroshio sites. Data from the Yellow Sea and the ECS were divided into three groups: Yellow Sea–ECS shelf sites at depths shallower than 150 m, Okinawa Trough sites deeper than 150 m, and off-Kyushu sites influenced by local freshwater inputs from Kyushu (Fig. 4 and Table 1). Given that the eastward-flowing CDW mixes with the warmer, more saline Kuroshio water near the shelf edge in the summer (Chang and Isobe 2003), salinity and $\delta^{18}O_{sw}$ values in the Kuroshio surface water should reflect the end-member for saline water (Kang et al. 1994). Therefore,

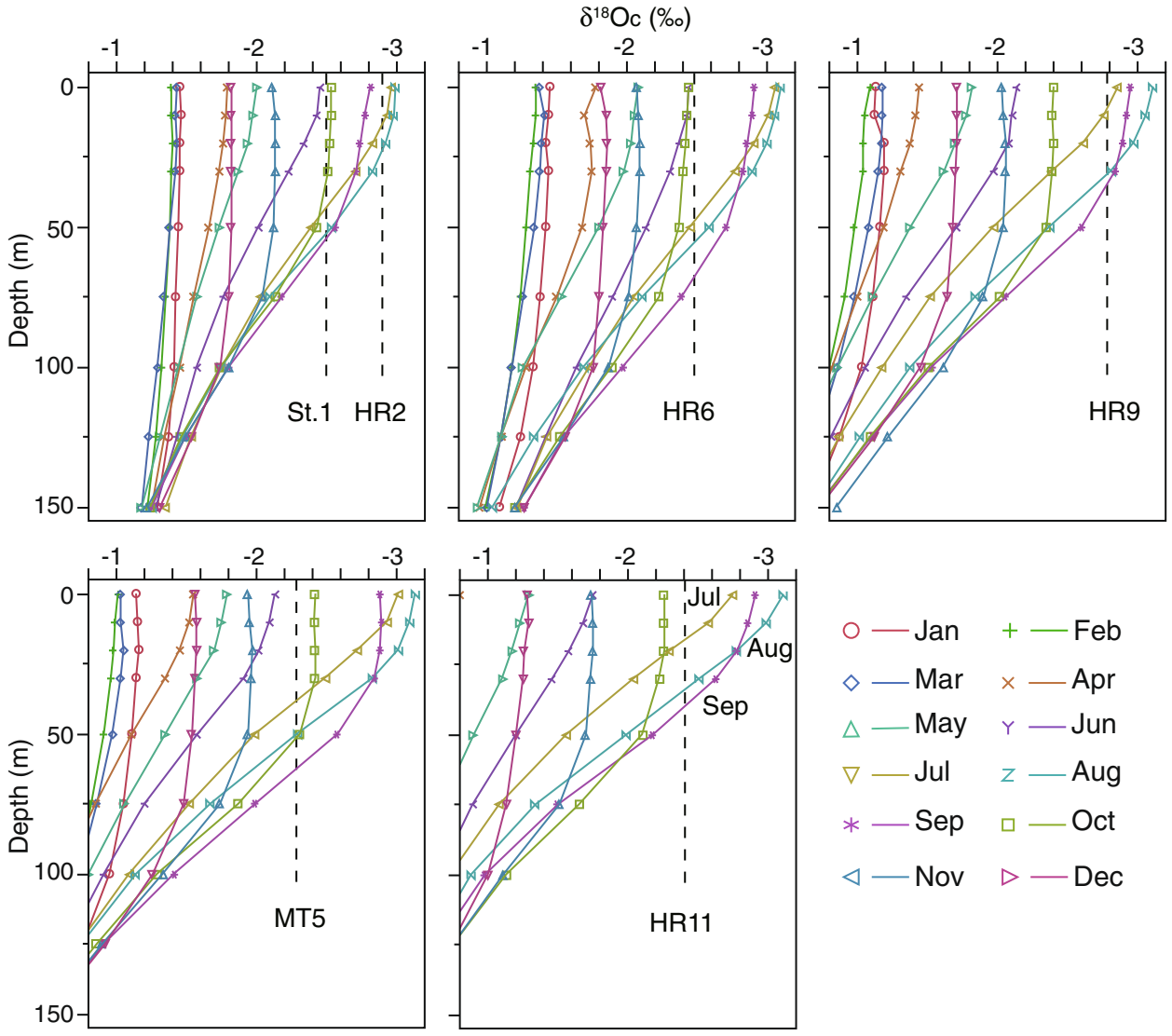

Fig. 5 Comparison of monthly variation in the predicted $\delta^{18}O_c$ values with the core-top $\delta^{18}O_c$ values. The *solid lines* show the monthly variation of the predicted $\delta^{18}O_c$ values within the water column. The *dotted lines* show the core-top $\delta^{18}O_c$ values of *G. ruber*. The predicted $\delta^{18}O_c$ values are calculated from temperature and salinity data (http://www.jodc.go.jp/) using a calcite equilibrium equation (Bemis et al. 1998). See details in the text

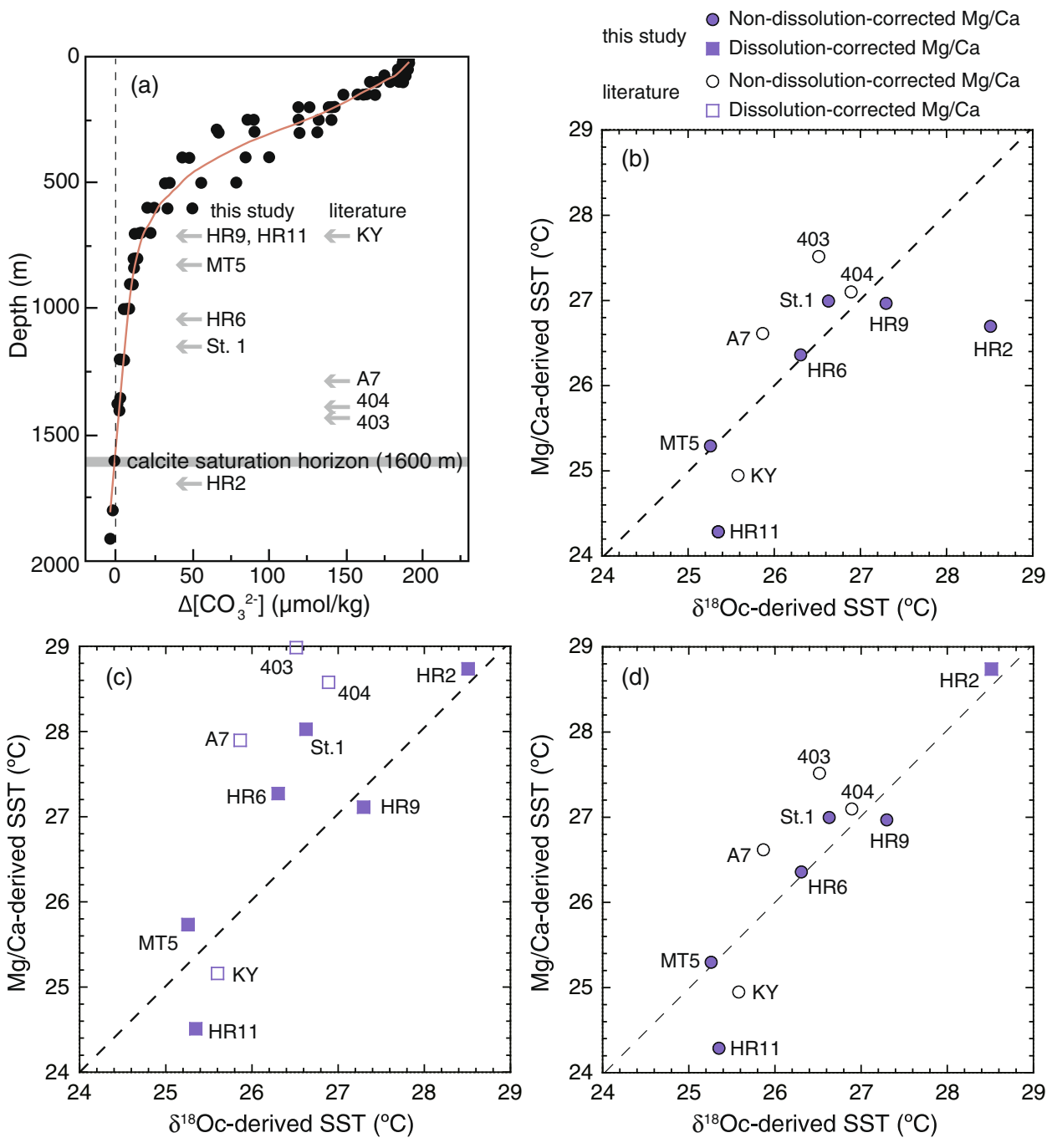

Fig. 6 Comparison of $\delta^{18}O_c$-derived calcification temperature with Mg/Ca-derived temperature. **a** Water column profile of $\Delta[CO_3^{2-}]$ in the ECS. Calculation of the calcite saturation state $\Delta[CO_3^{2-}]$ was accomplished via subtracting the carbonate ion concentration $[CO_3^{2-}]$ at saturation from the in situ $[CO_3^{2-}]$. To compute the in situ $[CO_3^{2-}]$ with the program CO2sys.xls (Lewis and Wallace 1998), we used total alkalinity, TCO_2, pH, and hydrographic water column data in the ECS (NODC Accession 0109919, http://data.nodc.noaa.gov/nodc/archive/metadata/approved/). *Arrows* indicate the water depths of cores analyzed in this study and by Sun et al. (2005), Lin et al. (2006), Chen et al. (2010), and Kubota et al. (2010). **b** $\delta^{18}O_c$-derived calcification temperature and non-dissolution-corrected Mg/Ca-derived temperature plot. **c** $\delta^{18}O_c$-derived calcification temperature and dissolution-corrected Mg/Ca-derived temperature plot. **d** $\delta^{18}O_c$-derived calcification temperature and Mg/Ca-derived temperature plot. The dissolution-corrected Mg/Ca ratio was used for the deepest site, HR2, where $\Delta[CO_3^{2-}] < 0$ μmol kg^{-1}. The other data were non-dissolution-corrected Mg/Ca ratios

taking into consideration this mixing of two water masses in the eastern part of the ECS, we derived the following $\delta^{18}O_{sw}$–salinity equation from the summer Yellow Sea–ECS shelf and Kuroshio site data:

$$\delta^{18}O_{sw} = -7.74\,(\pm 0.4) + 0.23\,(\pm 0.01) \times salinity\,\left(r^2 = 0.97, p < 0.001, n = 40\right) \quad (1)$$

The quoted errors of the slope and intercept are 95 % confidence intervals. This equation includes the surface (0–30 m water depth) and subsurface (40–100 m water depth) data. The surface data (0–30 m) alone result in the same equation within the 95 % confidence intervals of Eq. (1).

Equation (1) indicates a projected freshwater end-member of −7.74 ‰ (±0.4 ‰). This value is consistent with the $\delta^{18}O$ values (−8.4 to −7.1 ‰) for Changjiang River water in January and July (Zhang et al. 1990). However, the regression lines of the $\delta^{18}O_{sw}$–salinity relationships developed for the Changjiang River mouth and the western part of the ECS indicate lower $\delta^{18}O_{sw}$ values in the salinity range of 30 to 34 [$\delta^{18}O_{sw} = -8.41 + 0.24 \times$ salinity in January (line IV of Fig. 4) and $\delta^{18}O_{sw} = -7.06 + 0.20 \times$ salinity in July (line III of Fig. 4)]. Similar regression lines were developed for the Yellow Sea and the ECS [$\delta^{18}O_{sw} = -8.66 + 0.24 \times$ salinity in winter (line V of Fig. 4) and $\delta^{18}O_{sw} = -10.7 + 0.27 \times$ salinity in summer] (Ye et al. 2014). These regression lines do not pass through the end-member values of the Kuroshio surface water (salinity = 34.2–34.4 and $\delta^{18}O_{sw}$ = 0.1–0.2 ‰), indicating that the Kuroshio surface water was not the source of saline water for these areas (Fig. 4). Since these data were mainly from coastal and shelf waters near the Changjiang Estuary, the less saline, $\delta^{18}O$-depleted TWWC may be the dominant source of saline water rather than the Kuroshio water. Therefore, $\delta^{18}O_{sw}$–salinity relationships in the coastal ECS are highly variable and differ from our equation.

Like our regression line, regression lines that pass through the saline Kuroshio surface water were derived for the ECS shelf covering a broad sampling area for June–July (line II of Fig. 4) (Du et al. 2012), for the southern Yellow Sea in July (Kang et al. 1994), and for the area from the ECS to off the southern Japan Islands (Oba 1990) (line I of Fig. 4). Our regression line occupied an intermediate area between these regression lines. Furthermore, our equation is derived from the data obtained in the eastern part of the ECS where the eastward-flowing CDW mixes with the Kuroshio water in the summer. Therefore, our $\delta^{18}O_{sw}$–salinity equation should be representative of the northern Okinawa Trough during the EASM season.

Even if the freshwater end-member changed from −7.74 to −9.0 ‰ (given the averaged *y*-intercept of lines II, IV, and V as the potential change in the riverine $\delta^{18}O$), this change in amplitude does not yield a significant difference between the two calibration lines within the salinity range of 33 to 34.2. In addition, since end-member values of the CDW and the Kuroshio surface water may not have changed significantly during the Holocene in comparison with the glacial–interglacial cycles (Wang et al. 2008), our local $\delta^{18}O_{sw}$–salinity equation may provide an approximate relationship between the salinity and $\delta^{18}O_{sw}$ in the eastern part of the ECS, at least during the Holocene.

Core-top $\delta^{18}O_c$ and Mg/Ca ratios for *G. ruber*

The core-top $\delta^{18}O_c$ values for *G. ruber* ranged from −2.9 to −2.3 ‰ in the central to northern parts of the Okinawa Trough (Fig. 1 and Table 2). The lightest value was observed at HR2, the southernmost site, whereas the heaviest value was found at MT5 near the CDW advection area. Core-top Mg/Ca ratios of *G. ruber* ranged from 3.29 to 4.35 mmol mol^{-1} (Table 2). The Mg/Ca value at HR2 (4.09 mmol mol^{-1}, 1675 m water depth), which is the deepest site, was lower than that at the nearby shallower site St.1 (4.20 mmol mol^{-1}, 1153 m), even though HR2 had the lowest $\delta^{18}O_c$ value of *G. ruber* (−2.9 ‰) (Table 2). Since site HR2 is below the CSH (~1600 m) (Fig. 6a), the Mg/Ca ratio at HR2 seems to be lowered due to calcite dissolution (discussed below). Core-top Mg/Ca ratios, including the data from the literature (Sun et al. 2005; Lin et al. 2006; Chen et al. 2010; Kubota et al. 2010), tend to be higher in the southern sites (e.g., HR2 and St.1) and lower in the northern sites (HR11 and MT5) (Table 2), which is consistent with the distribution of the summer SST. In contrast, core-top $\delta^{18}O_c$ values correlate poorly with the Mg/Ca ratios ($r^2 = 0.19$), indicating that $\delta^{18}O_c$ values are strongly influenced by $\delta^{18}O_{sw}$.

Calcification season and calcification temperature of *G. ruber*

The foraminifera shell Mg/Ca response to temperature is biologically modulated and dependent on pH and/or $[CO_3^{2-}]$ (Lea et al. 1999; Russell et al. 2004). Therefore, many species- and basin-specific Mg/Ca–temperature equations have been developed, some of which take into consideration the potential effect of dissolution (Lea et al. 2000; Dekens et al. 2002; Anand et al. 2003; McConnell and Thunell 2005). There is, however, no equation for *G. ruber* in the ECS, and previous studies conducted in the ECS have converted Mg/Ca values of *G. ruber* to SST using a Mg/Ca–temperature calibration equation [T (°C) = ln(Mg/Ca/0.38)/0.089] developed for *G. ruber* based on the SCS core-top sediments by Hastings et al. (2001) (Sun et al. 2005; Lin et al. 2006; Chen et al. 2010; Kubota et al. 2010). Although this calibration equation yields temperatures corresponding to the warm

summer months, it has not been fully investigated whether there is consistency between $\delta^{18}O_c$- and Mg/Ca-derived temperatures, even though reconciled estimates of temperatures are crucial for calculating $\delta^{18}O_{sw}$.

First, to calculate calcification temperatures ($\delta^{18}O_c$-derived SSTs), we identified the calcification season and depth based on a comparison of core-top $\delta^{18}O_c$ values with predicted $\delta^{18}O_c$ values. Predicted $\delta^{18}O_c$ values were calculated using the following $\delta^{18}O_c$–temperature equation assuming oxygen isotopic equilibrium in foraminiferal calcite:

$$T(^\circ\mathrm{C}) = 14.9 - 4.8\left(\delta^{18}O_c - \left(\delta^{18}O_{sw} - 0.27‰\right)\right) \quad (2)$$

This $\delta^{18}O_c$–temperature equation was determined from culturing experiments of a symbiont-bearing species, *Orbulina universa*, grown under high-light conditions (Bemis et al. 1998). The high-light conditions (>380 μEinstein m^{-2} s^{-1}) in the culturing experiments take into consideration symbiont effects on shell $\delta^{18}O_c$ (i.e., high photosynthetic activity forms ^{18}O-depleted shells). The applicability of this equation to the surface-dwelling, symbiont-bearing species *G. ruber* has been confirmed (Bemis et al. 1998; Benway et al. 2006). Temperature and salinity data averaged statistically for 1930–2003 in a 1° × 1° (latitude × longitude) grid provided by JODC were used for the calculation. Salinity was converted to $\delta^{18}O_{sw}$ values using Eq. (1). The term −0.27 ‰ corrects for the $\delta^{18}O$ difference between VSMOW and Pee Dee Belemnite (PDB).

Figure 5 shows a comparison of the predicted vertical profiles of $\delta^{18}O_c$ values for each month with core-top $\delta^{18}O_c$ values of *G. ruber* at each site. Among the six core-top datasets, HR2 and HR9 showed relatively lighter $\delta^{18}O_c$ values that are approximately equal to the $\delta^{18}O_c$ values in the surface water for July–September. In contrast, the other sites (St.1, HR6, MT5, and HR11) were marked by isotopically heavier values than the peak summer $\delta^{18}O_c$ in the surface water, suggesting a large contribution of *G. ruber* shells formed in deeper waters (>50 m) or in surface water in May, June, and/or October (Fig. 5). Since *G. ruber* (sensu stricto) lives predominantly in the top 20 m of the subtropical North Pacific (Kuroyanagi and Kawahata 2004), calcification of shells in deeper water (>50 m) should be negligible. Furthermore, sediment trap data from the ECS, which unfortunately do not include data for September, show that the fluxes of *G. ruber* from May to October account for 80 % of the total fluxes each year and the fluxes in May alone account for 20 % of the yearly fluxes (Xu et al. 2005). Based on these data, we regard the dominant habitat depth of *G. ruber* in the ECS as the top 0 to 30 m (mixed layer) and contend that the *G. ruber* shell geochemistry in the ECS records the weighted mean surface ocean conditions from May to October.

To calculate the calcification temperatures and salinity of the seawater in which *G. ruber* shells were formed, we computed seasonal average (May–October or July–September) $\delta^{18}O_c$ values and compared these predicted values to core-top $\delta^{18}O_c$ values (Table 2). The calcification seasons and depths at HR2 and HR11 were identified as July–September and 0–10 m and June–September and 0–30 m, respectively. The $\delta^{18}O_c$-derived SSTs at HR2 and HR11 were calculated as 28.5 and 25.3 °C, respectively (Fig. 6 and Table 2). The calculated calcification SSTs at all sites ranged from 25.1 to 28.5 °C in the central to northern Okinawa Trough (Table 2). It is noteworthy that the calcification season of *G. ruber* was not necessarily uniform across the ECS; data from sites HR2 and HR9 clearly show a warmer seasonal bias (close to the peak summer SST), in contrast to other site data (Figs. 1 and 5). The core-top $\delta^{18}O_c$ data shows that Eq. (2) provides better estimates for calcification depth, season, and temperature that agree with sediment trap and plankton tow data (Kuroyanagi and Kawahata 2004; Xu et al. 2005).

Although we applied the $\delta^{18}O_c$–temperature equation by Bemis et al. (1998) to the core-top data, there are other $\delta^{18}O_c$–temperature relationships that yield various estimates for calcification temperature. For instance, $\delta^{18}O_c$–temperature equations by Kim and O'Neil (1997) and Mulitza et al. (2003) yield an offset of approximately 1 °C to the calcification temperatures calculated by Eq. (2). If these equations are applied to our core-top data with the assumption of $\delta^{18}O$ equilibrium, calcification temperatures at HR2 and HR9 will exceed the peak summer SST. Therefore, we should consider $\delta^{18}O$ disequilibrium in foraminiferal calcite (i.e., vital effect) for at least these sites. However, since the vital effect for *G. ruber* has not been determined precisely (0 to −1.0 ‰) (Niebler et al. 1999), applying these equations will introduce significant uncertainties in calcification temperature estimates.

Assessment of *G. ruber* Mg/Ca-derived temperatures

G. ruber is one of the species of planktonic foraminifera most susceptible to dissolution (Thunell and Honjo 1981). Partial dissolution of *G. ruber* shells can decrease Mg/Ca ratios owing to the higher solubility of Mg-rich calcite (Dekens et al. 2002). The ECS is the most undersaturated marginal sea with respect to calcite, and the CSH is shallow (~1600 m) (Fig. 6a). In our dataset, site HR2 is below the CSH, and the published core-top data from site A7, MD012404 (hereafter 404), and MD012403 (hereafter 403) were also derived from bottom water conditions with low calcite saturation states of <5 μmol kg^{-1} ($\Delta[CO_3^{2-}] = [CO_3^{2-}]_{in\ \ situ} - [CO_3^{2-}]_{saturation}$) (Fig. 6a; see

caption of Fig. 6a for more details). According to data from core-top *G. ruber* tests of a depth transect in the Ontong Java Plateau, Mg/Ca ratios of *G. ruber* started to decrease with decreasing $\Delta[CO_3^{2-}]$ (–0.05 mmol mol^{-1} per μmol^{-1} kg^{-1}) from an initial $\Delta[CO_3^{2-}]$ of 14 μmol kg^{-1} (Johnstone et al. 2011). This finding is a cause for concern that ECS Mg/Ca data obtained under bottom water conditions with low $\Delta[CO_3^{2-}]$ may be influenced by dissolution (Fig. 6a).

Therefore, we assessed the impact of calcite dissolution on Mg/Ca ratios in the ECS by applying critical thresholds for the dissolution (14 μmol kg^{-1} $\Delta[CO_3^{2-}]$) and the sensitivity of the Mg/Ca ratio to $\Delta[CO_3^{2-}]$ (0.05 mmol mol^{-1} per μmol^{-1} kg^{-1}) (Johnstone et al. 2011). We calculated $\Delta[CO_3^{2-}]$ for the bottom waters at each core site and estimated the dissolution-corrected Mg/Ca ratios for all core sites (Table 2). Figure 6 shows a comparison of the $\delta^{18}O_c$-derived SSTs with non-dissolution-corrected and dissolution-corrected Mg/Ca-derived SSTs (Fig. 6b, c). Both Mg/Ca ratios were converted to SSTs using the SCS calibration equation of Hastings et al. (2001).

The shallowest site, HR9, where the $\Delta[CO_3^{2-}]$ value is 12.9 μmol kg^{-1}, showed good agreement with the non-dissolution-corrected Mg/Ca- and $\delta^{18}O_c$-derived SSTs (Fig. 6b). It is noteworthy that core-top data at depths ranging from 1000 to ~1400 m (HR6, St.1, A7, 404, and 403) also showed agreement with the non-dissolution-corrected Mg/Ca- and $\delta^{18}O_c$-derived SSTs, even though the $\Delta[CO_3^{2-}]$ values were lower than the critical threshold for dissolution (10–20 μmol kg^{-1}) (Regenberg et al. 2009; Johnstone et al. 2011) (Fig. 6b). The deepest site, HR2 (1675 m water depth), showed that the non-dissolution-corrected Mg/Ca-derived SST underestimates the $\delta^{18}O_c$-derived SST by 1.8 °C (Fig. 6b), and the dissolution-corrected Mg/Ca-derived SST agrees well with the $\delta^{18}O_c$-derived SST (Fig. 6c). However, this dissolution correction induced a larger offset to the $\delta^{18}O_c$-derived SSTs for other sites (1000 to ~1400 m water depths) (Fig. 6c).

The Mg/Ca–temperature calibration equation of Hastings et al. (2001) was developed for *G. ruber* from SCS core-top samples recovered from depths above 2000 m. As in the ECS, the deep waters in the SCS are characterized by low $\Delta[CO_3^{2-}]$ with the CSH at a water depth of 2500 m (Regenberg et al. 2009). Presumably, samples recovered from depths of 1500 to 2000 m (<15 μmol kg^{-1} $\Delta[CO_3^{2-}]$) for the calibration equation might have been influenced by partial dissolution under low $\Delta[CO_3^{2-}]$. Therefore, we consider that the SCS calibration equation potentially involves a correction for calcite dissolution under low $\Delta[CO_3^{2-}]$. Consequently, the correction for calcite dissolution is required only for samples obtained below the CSH in the ECS.

Thus, in this study, we integrated data of dissolution-corrected (for HR2 from below the CSH) and non-dissolution-corrected (for other cores above the CSH) Mg/Ca values to obtain Mg/Ca-derived SSTs (Fig. 6d). Although HR11 and 403 are still offset from the $\delta^{18}O_c$-derived SST by 1 °C, the other core-top data showed good agreement with both SST estimates ($r^2 = 0.83$, $p < 0.001$, except HR11 and 403) (Fig. 6d). This SCS calibration equation reconciles Mg/Ca-derived and $\delta^{18}O_c$-derived SSTs in the ECS, both of which reflect SSTs in the warmer season months. However, other calibration equations (Lea et al. 2000; Anand et al. 2003; McConnell and Thunell 2005) do not yield temperatures corresponding to the warmer season months and do not agree well with $\delta^{18}O_c$-derived SSTs (Table 2).

$\delta^{18}O_{sw}$ estimate for *G. ruber* in core-top sediments

Core-top $\delta^{18}O_{sw}$ values were calculated from Mg/Ca-derived SSTs and core-top $\delta^{18}O_c$ values using Eq. (2). The core-top data of the shell-derived $\delta^{18}O_{sw}$ and the salinity, including the published data from KY, A7, 404, and 403 (Sun et al. 2005; Lin et al. 2006; Chen et al. 2010; Kubota et al. 2010), are plotted in Fig. 7a. Since the estimation of the shell-derived $\delta^{18}O_{sw}$ is affected by the uncertainty in the $\delta^{18}O_c$ (±0.11 ‰) and the Mg/Ca-derived temperature (±1 °C, corresponding to approximately ±0.26 ‰) (Schmidt 1999; Rohling 2007), the reconstructed $\delta^{18}O_{sw}$ introduces a large propagation error of ±0.28 ‰ (1σ). Although the regression line of the core-top $\delta^{18}O_{sw}$ data has a steeper gradient and a lower y-intercept, given 1σ error bars of $\delta^{18}O_{sw}$ estimates the data points fall primarily on the local $\delta^{18}O_{sw}$–salinity regression line of the eastern part of the ECS (Fig. 7a). Indeed, sites KY and HR11 in the northern Okinawa Trough were marked by the lowest shell-derived $\delta^{18}O_{sw}$ values, whereas St.1 and A7 in the central Okinawa Trough showed the highest shell-derived $\delta^{18}O_{sw}$ values. Sites HR9 and MT5 had intermediate $\delta^{18}O_{sw}$ values between the above two datasets (Fig. 7a). The core-top $\delta^{18}O_{sw}$ values were roughly distributed as expected from the peak summer SSS at each site.

Although site MT5 is in an area with a lower summer SSS than that of site HR9, the shell-derived $\delta^{18}O_{sw}$ value at MT5 (0.17 ‰) was higher than that at HR9 (0.01 ‰) (Fig. 7a). One potential explanation is that *G. ruber* shells at HR9 were formed in the surface waters during the peak summer season when SSS decreases distinctly, whereas *G. ruber* at MT5 was not abundant in the peak summer season, as inferred from the $\delta^{18}O_c$ data (Fig. 5). These data tell us that the difference of 0.16 ‰ in the shell-derived $\delta^{18}O_{sw}$ may be caused by changes in the seasonal habitat of *G. ruber*.

This core-top investigation shows that realistic $\delta^{18}O_{sw}$ values can be reconstructed by the Mg/Ca–temperature calibration of Hastings et al. (2001) and the $\delta^{18}O_c$–

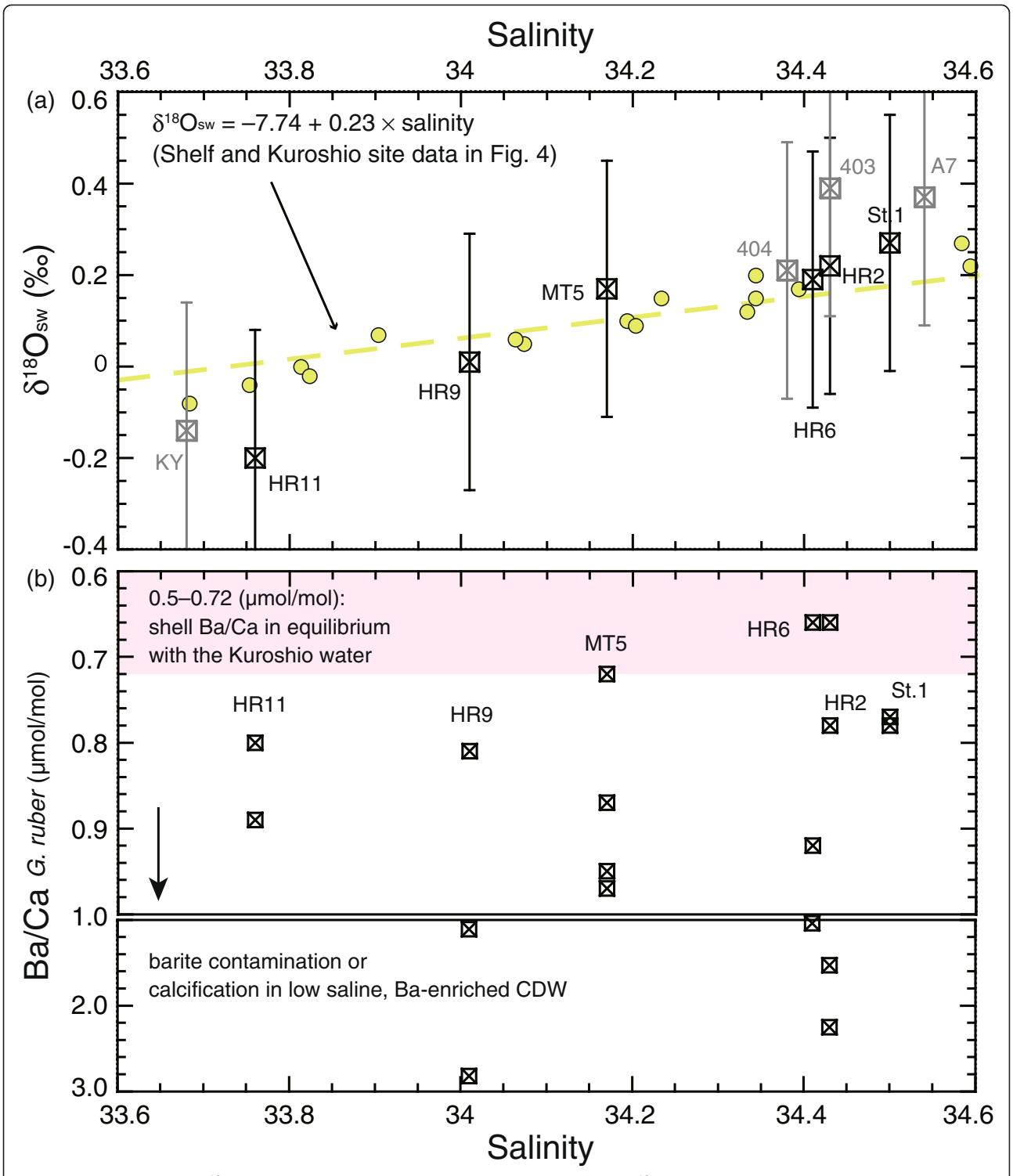

Fig. 7 Salinity, shell-derived $\delta^{18}O_{sw}$, and Ba/Ca ratios of core-top *G. ruber* tests. **a** Shell-derived $\delta^{18}O_{sw}$ and calcification salinity plot of core-top samples in this study and the literature. Shell-derived $\delta^{18}O_{sw}$ values are calculated using the Mg/Ca-derived temperature and core-top $\delta^{18}O_c$ of *G. ruber*. The data from KY, A7, 403, and 404 (*gray squares*) are from Kubota et al. (2010), Sun et al. (2005), Lin et al. (2006), and Chen et al. (2010), respectively. *Error bars* show the propagation error of ±0.28 ‰ (1σ). Seawater data (*green circles*) and their regression line (green broken line, Fig. 4) are also shown with the core-top data. Core-top data fall close to the local $\delta^{18}O_{sw}$–salinity regression line. **b** $Ba/Ca_{G.\ ruber}$ ratios and calcification salinity plot of all core-top samples in this study. The replicated analyses of $Ba/Ca_{G.\ ruber}$ ratios at each core site show high variability, resulting in the range from 0.66 to 2.82 μmol mol^{-1}. The calculated shell Ba/Ca ratio in equilibrium with the Kuroshio water is 0.5–0.72 μmol mol^{-1}. Lower values at HR2 and HR6 are within this range. Higher shell Ba/Ca ratios than this Kuroshio water range might be attributable to barite contamination or calcification in low saline, Ba-enriched CDW

temperature equation of Bemis et al. (1998), although $\delta^{18}O_{sw}$ estimates introduce a large error. Furthermore, this finding indicates that robust reconstruction of EASM-related variability in SSS might be possible by conducting multiple replicates of paired $\delta^{18}O_c$ and Mg/Ca analyses to decrease the large uncertainty. In addition, the utility of potential paleo-salinity proxies, such as the foraminiferal Ba/Ca ratio and the organic compound-specific δD, should be investigated further (Rohling 2007).

Possibility of using Ba/Ca ratios of *G. ruber* as a proxy for surface salinity

In general, the desorption of Ba^{2+} from suspended sediments in rivers results in a very high riverine [Ba^{2+}] relative to seawater. If there is a single river source, conservative mixing of river water and ambient seawater produces a linear inverse correlation between salinity and [Ba^{2+}] (Bahr et al. 2013). Ba^{2+} incorporation into living planktonic foraminifera shells is linearly dependent on the [Ba^{2+}] of the water, with a constant partition coefficient for Ba ($D_{Ba} = 0.15$) (Lea and Spero 1994; Hönisch et al. 2011). *G. ruber* populations can thrive in low-salinity surface water influenced by river discharge (Schmuker and Schiebel 2002; Arnold and Parker 2003). This ecological preference of *G. ruber* and the incorporation of Ba into foraminifera shells makes Ba/Ca ratios in fossil *G. ruber* a proxy for the influence of river discharge on salinity (Weldeab et al. 2007; Schmidt and Lynch-Stieglitz 2011).

In the case of the ECS, the Changjiang River accounts for approximately 90 % of the total river discharge into the ECS, with large quantities of Ba^{2+} (~360 nmol L^{-1}) (Beardsley et al. 1985; Qu et al. 1993; Yanagi 1994). Based on our preliminary [Ba^{2+}] data in the ECS measured by an isotope dilution method (Klinkhammer and Chan 1990), the surface water at SSW8 (30.80 salinity) showed a high [Ba^{2+}] of 57.0 nmol L^{-1} (Ba/Ca ratio of 6.31 μmol mol^{-1}), and the Kuroshio surface water (SSW14–17, average 34.2) showed a low [Ba^{2+}] of 32.9 nmol L^{-1} (Ba/Ca of 3.27 μmol mol^{-1}). The [Ba^{2+}] data for the Kuroshio water were consistent with previously reported data from Kuroshio waters (29.9–33.5 nmol L^{-1}) (Sugiyama et al. 1984). Other surface samples from the northern Okinawa Trough fall within these [Ba^{2+}] and Ba/Ca ranges, showing a linear relationship between $Ba/Ca_{seawater}$ and salinity (Horikawa et al., personal communication).

Our Ba/Ca ratios in *G. ruber* (hereafter $Ba/Ca_{G.\ ruber}$) from core-top sediments ranged from 0.66 to 2.82 μmol mol^{-1} (Fig. 7b). The lowest Ba/Ca value of 0.66 μmol mol^{-1} was observed at sites HR2 and HR6 in the central Okinawa Trough. Given the $Ba/Ca_{seawater}$ ratio of 3.27 μmol mol^{-1} in the Kuroshio surface water and the likely D_{Ba} of 0.15–0.22 (Hall and Chan 2004; Hönisch et al. 2011), the calculated shell Ba/Ca ratio in equilibrium with the Kuroshio water should be 0.5 to 0.72 μmol mol^{-1}. Indeed, HR2 and HR6 values were within the expected range for Kuroshio surface water. In contrast, HR11, where the lowest SSS among the studied sites was observed, had relatively higher $Ba/Ca_{G.\ ruber}$ ratios (0.80–0.89 μmol mol^{-1}) (Fig. 7b). Given the $Ba/Ca_{seawater}$ ratio of 3.8 μmol mol^{-1} (at HR10, 0 m) and the D_{Ba} of 0.15 to 0.22, the shell Ba/Ca ratio in equilibrium should be 0.57 to 0.84 μmol mol^{-1}. The core-top $Ba/Ca_{G.\ ruber}$ ratios observed at HR11 were consistent with the upper range of expected values, probably reflecting the influence of the Ba-enriched CDW (i.e., low-salinity waters).

However, all core-top $Ba/Ca_{G.\ ruber}$ data at six sites do not show a significant relationship with the salinity, but replicate data at each site showed highly variable $Ba/Ca_{G.\ ruber}$ ratios, some of which exceeded the values at site HR11 (Fig. 7b). Although we are unable to adequately explain such highly variable $Ba/Ca_{G.\ ruber}$ ratios at this time, one likely reason is sample heterogeneity. In this study, to obtain averaged $Ba/Ca_{G.\ ruber}$ ratios for each site, we re-picked 20–30 shells of *G. ruber* more than twice after picking the samples labeled run #1 (Table 2). Although the samples from run #1 gave reasonable $Ba/Ca_{G.\ ruber}$ ratios (0.66–0.89 μmol mol^{-1}) at each site except HR6, the samples from runs #2 to #4 yielded anomalously high $Ba/Ca_{G.\ ruber}$ ratios compared with the samples from run #1. Given that there were few well-preserved, clean *G. ruber* tests for these sites and that replicate measurements of Mn/Ca and Mg/Ca ratios were within an acceptable range, we argue that samples from runs #2 to #4 may have involved impure *G. ruber* tests in which barite crystallized on fossil shell surfaces.

Finally, based on the available dataset of $Ba/Ca_{seawater}$ in the ECS, we propose that pristine $Ba/Ca_{G.\ ruber}$ ratios at northern Okinawa Trough sites would be less than 0.84 μmol mol^{-1}. A possible reason for higher core-top $Ba/Ca_{G.\ ruber}$ ratios (>0.84 μmol mol^{-1}) is contamination by sedimentary barite adherent on fossil shells. Our preliminary data suggest that $Ba/Ca_{G.\ ruber}$ data as a paleo-salinity proxy should be derived from well-preserved, clean *G. ruber* tests or diethylene triamine pentaacetic acid (DTPA)-cleaned *G. ruber* tests that can minimize the influence of barite contamination (Lea and Boyle 1991; Hall and Chan 2004). Since the $Ba/Ca_{G.\ ruber}$ records from the northern Okinawa Trough sediments may potentially identify high river discharge events related to stronger EASMs, assessment of foraminiferal Ba/Ca should be continued in the ECS.

Conclusions

The main findings of this study are as follows:

(1) Shallow seawater samples (0–100 m) taken from the ECS in early July showed a strong correlation between $\delta^{18}O_{sw}$ and salinity. The *T*–*S* diagram in the surface waters in the ECS shows that the eastward-flowing CDW mixes with the saline Kuroshio waters. Based on this finding, we derived the following $\delta^{18}O_{sw}$–salinity equation from the Yellow Sea–ECS shelf and Kuroshio site data:

$$\delta^{18}O_{sw} = -7.74(\pm 0.4) + 0.23(\pm 0.01) \times salinity\left(r^2 = 0.97, p < 0.001, n = 40\right).$$

This local $\delta^{18}O_{sw}$–salinity equation might be representative of the northern Okinawa Trough during the EASM season.

(2) We found that the dominant habitat depth of *G. ruber* is within the top 0 to 30 m in the ECS. The calcification season of *G. ruber* is mainly during the warm summer months (May–October) but may not necessarily be uniform across the ECS. We confirmed that the Mg/Ca–temperature calibration by Hastings et al. (2001) yields temperatures corresponding to the warmer season months, as expected from sediment trap data. The Mg/Ca-derived SSTs agreed with calcification temperatures calculated by Bemis et al. (1998). Site HR2, where the bottom water is undersaturated with calcite, required a correction for calcite dissolution.

(3) We found that core-top data for shell-derived $\delta^{18}O_{sw}$ and salinity fall primarily on our local $\delta^{18}O_{sw}$–salinity regression line giving 1σ error of $\delta^{18}O_{sw}$ estimates. The Mg/Ca–temperature calibration by Hastings et al. (2001) and the $\delta^{18}O_c$–temperature equation by Bemis et al. (1998) should be appropriate for calculating $\delta^{18}O_{sw}$ in the ECS.

(4) $Ba/Ca_{G.\ ruber}$ from core-top sediments ranged from 0.66 to 2.82 μmol mol^{-1}. There was not a significant relationship between salinity and $Ba/Ca_{G.\ ruber}$ due to the highly variable $Ba/Ca_{G.\ ruber}$ data. Given the seawater Ba/Ca data and the published partition coefficient for Ba (D_{Ba} = 0.15–0.22), pristine $Ba/Ca_{G.\ ruber}$ ratios at northern Okinawa Trough sites should be less than 0.84 μmol mol^{-1}. One possible reason for higher $Ba/Ca_{G.\ ruber}$ ratios (>0.84 μmol mol^{-1}) is contamination by sedimentary barite adherent on fossil shells. Further evaluation of the $Ba/Ca_{G.\ ruber}$ ratio as a paleo-salinity proxy requires DTPA-cleaned Ba/Ca data that can minimize the influence of barite contamination.

Abbreviations

EASM: East Asian summer monsoon; ECS: East China Sea; CDW: Changjiang diluted water; SSS: sea surface salinity; TWWC: Taiwan warm current; SCS: South China Sea; YSCCW: Yellow Sea Central Cold Water; SST: sea surface temperature; JODC: Japan Oceanographic Data Center; CTD: conductivity, temperature, and depth; JGOFS: Joint Global Ocean Flux Study; IAPSO: International Association for the Physical Sciences of the Oceans; CSH: calcite saturation horizon; VSMOW: Vienna Standard Mean Ocean Water; CMCR: Center for Advanced Marine Core Research; PDB: Pee Dee Belemnite; DTPA: diethylene triamine pentaacetic acid.

Competing interests

The authors declare that they have no competing interests.

Authors' contributions

KH conceived and designed the study. TK carried out the measurements of the seawater $\delta^{18}O$, foraminiferal $\delta^{18}O_c$, and metal/Ca ratios under the supervision of Professors MM and JZ. All authors analyzed and discussed the data. All authors contributed toward writing the manuscript and read and approved the final manuscript.

Authors' information

KH is an associate professor at the University of Toyama. He is a paleoceanographer and a geochemist who has worked on SST reconstruction around Japan using the Mg/Ca–temperature proxy and the analysis of deep-sea water mass circulation using neodymium isotopes. JZ is also a geochemist and a professor at the University of Toyama with considerable experience in geochemical analysis. TK is a Ph.D. student supervised by KH and JZ. MM is a professor at the Center for Advanced Marine Core Research (CMCR), Kochi University.

Acknowledgements

We acknowledge the tremendous support of the KH-13-4 and KT-12-25 shipboard scientists and staff. This study was performed under the cooperative research program of the Center for Advanced Marine Core Research (CMCR), Kochi University (#13B050). We thank the chief editors Ryuji Tada, Hodaka Kawahata, Yasufumi Iryu, and two anonymous reviewers for their significant help in improving this manuscript.

Author details

[1]Graduate School of Science and Engineering for Research, University of Toyama, Gofuku 3190, Toyama 930-8555, Japan. [2]Graduate School of Science and Engineering for Education, University of Toyama, Gofuku 3190, Toyama 930-8555, Japan. [3]Center for Advanced Marine Core Research, Kochi University, B200 Monobe, Nankoku 783-8502, Japan.

Received: 30 September 2014 Accepted: 25 May 2015
Published online: 07 July 2015

References

Anand P, Elderfield H, Conte MH (2003) Calibration of Mg/Ca thermometry in planktonic foraminifera from a sediment trap time series. Paleoceanography 18(2):1050. doi:10.1029/2002PA000846

Arnold A, Parker W (2003) Biogeography of planktonic Foraminifera. In: Gupta BKS (ed) Modern Foraminifera. Springer, Netherlands, pp 103–122. doi:10.1007/0-306-48104-9_7

Bahr A, Schönfeld J, Hoffmann J, Voigt S, Aurahs R, Kucera M, Flögel S, Jentzen A, Gerdes A (2013) Comparison of Ba/Ca and $\delta^{18}O_{WATER}$ as freshwater proxies: A multi-species core-top study on planktonic foraminifera from the vicinity of the Orinoco River mouth. Earth Planet Sci Lett 383:45–57. doi:10.1016/j.epsl.2013.09.036

Beardsley RC, Limeburner R, Yu H, Cannon GA (1985) Discharge of the Changjiang (Yangtze River) into the East China Sea. Cont Shelf Res 4(1–2):57–76. doi:10.1016/0278-4343(85)90022-6

Bemis BE, Spero HJ, Bijima J, Lea DW (1998) Reevaluation of the oxygen isotopic composition of planktonic foraminifera: Experimental results and revised paleotemperature equations. Paleoceanography 13(2):150–160

Benway HM, Mix AC, Haley BA, Klinkhammer GP (2006) Eastern Pacific Warm Pool paleosalinity and climate variability: 0–30 kyr. Paleoceanography 21(3):PA3008. doi:10.1029/2005PA001208

Boyle EA, Keigwin LD (1985) Comparison of Atlantic and Pacific paleochemical records for the last 215,000 years: changes in deep ocean circulation and chemical inventories. Earth Planet Sci Lett 76(1–2):135–150

Chang P-H, Isobe A (2003) A numerical study on the Changjiang diluted water in the Yellow and East China Seas. J Geophys Res 108(C9):3299. doi:10.1029/2002JC001749

Chang Y-P, Chen M-T, Yokoyama Y, Matsuzaki H, Thompson WG, Kao S-J, Kawahata H (2009) Monsoon hydrography and productivity changes in the East China Sea during the past 100,000 years: Okinawa Trough evidence (MD012404). Paleoceanography 24(3):PA3208. doi:10.1029/2007PA001577

Chen C, Beardsley RC, Limeburner R, Kim K (1994) Comparison of winter and summer hydrographic observations in the Yellow and East China Seas and adjacent Kuroshio during 1986. Cont Shelf Res 14(7–8):909–929. doi:10.1016/0278-4343(94)90079-5

Chen F, Yu Z, Yang M, Ito E, Wang S, Madsen DB, Huang X, Zhao Y, Sato T, Birks HJB, Boomer I, Chen J, An C, Wünnemann B (2008) Holocene moisture evolution in arid central Asia and its out-of-phase relationship with Asian monsoon history. Quat Sci Rev 27(3–4):351–364. doi:10.1016/j.quascirev.2007.10.017

Chen MT, Lin XP, Chang YP, Chen YC, Lo L, Shen CC, Yokoyama Y, Oppo DW, Thompson WG, Zhang R (2010) Dynamic millennial-scale climate changes in the northwestern Pacific over the past 40,000 years. Geophys Res Lett 37(23):L23603. doi:10.1029/2010GL045202

Dekens PS, Lea DW, Pak DK, Spero HJ (2002) Core top calibration of Mg/Ca in tropical foraminifera: Refining paleotemperature estimation. Geochem Geophys Geosyst 3(4):1–29. doi:10.1029/2001GC000200

Du J, Chen M, Cao J, Qiu Y, Tong J, Ma Q, Yang J (2012) Oxygen isotope in seawater and its hydrological implication in the southern Yellow Sea and the East China Sea. Oceanol Limnol Sin 43(6):1057–1066 (in Chinese with English abstract)

Epstein S, Mayeda T (1953) Variation of O18 content of waters from natural sources. Geochim Cosmochim Acta 4(5):213–224. doi:10.1016/0016-7037(53)90051-9

Greaves M, Caillon N, Rebaubier H, Bartoli G, Bohaty S, Cacho I, Clarke L, Cooper M, Daunt C, Delaney M, deMenocal P, Dutton A, Eggins S, Elderfield H, Garbe-Schoenberg D, Goddard E, Green D, Groeneveld J, Hastings D, Hathorne E, Kimoto K, Klinkhammer G, Labeyrie L, Lea DW, Marchitto T, Martinez-Boti MA, Mortyn PG, Ni Y, Nuernberg D, Paradis G et al (2008) Interlaboratory comparison study of calibration standards for foraminiferal Mg/Ca thermometry. Geochem Geophys Geosyst 9(8):Q08010. doi:10.1029/2008gc001974

Hall JM, Chan LH (2004) Ba/Ca in Neogloboquadrina pachyderma as an indicator of deglacial meltwater discharge into the western Arctic Ocean. Paleoceanography 19(1):PA1017. doi:10.1029/2003PA000910

Hastings DW, Whitko A, Kienast M, Steinke S (2001) A comparison of three independent paleotemperature estimates from a high resolution record of deglacial SST records in the tropical South China Sea. Eos 82:PP12B–10

Hönisch B, Allen KA, Russell AD, Eggins SM, Bijma J, Spero HJ, Lea DW, Yu J (2011) Planktic foraminifers as recorders of seawater Ba/Ca. Mar Micropaleontol 79(1–2):52–57. doi:10.1016/j.marmicro.2011.01.003

Ichikawa H, Beardsley R (2002) The Current System in the Yellow and East China Seas. J Oceanogr 58(1):77–92. doi:10.1023/A:1015876701363

Jan S, Sheu DD, Kuo H-M (2006) Water mass and throughflow transport variability in the Taiwan Strait. J Geophys Res 111(C12):C12012. doi:10.1029/2006JC003656

Johnstone HJH, Yu J, Elderfield H, Schulz M (2011) Improving temperature estimates derived from Mg/Ca of planktonic foraminifera using X-ray computed tomography–based dissolution index, XDX. Paleoceanography 26(1):PA1215. doi:10.1029/2009PA001902

Kang D-J, Chung CS, Kim SH, Hong GH, Kim K-R (1994) Oxygen isotope characteristics of seawaters in the Yellow Sea. La mer 32:279–284

Kim S-T, O'Neil JR (1997) Equilibrium and nonequilibrium oxygen isotope effects in synthetic carbonates. Geochim Cosmochim Acta 61(16):3461–3475. doi:10.1016/S0016-7037(97)00169-5

Kim K-R, Cho Y-K, Kang D-J, Ki J-H (2005) The origin of the Tsushima Current based on oxygen isotope measurement. Geophys Res Lett 32(3):L03602. doi:10.1029/2004GL021211

Klinkhammer GP, Chan LH (1990) Determination of barium in marine waters by isotope dilution inductively coupled plasma mass spectrometry. Anal Chim Acta 232(0):323–329. doi:10.1016/S0003-2670(00)81249-0

Kubota Y, Kimoto K, Tada R, Oda H, Yokoyama Y, Matsuzaki H (2010) Variations of East Asian summer monsoon since the last deglaciation based on Mg/Ca and oxygen isotope of planktic foraminifera in the northern East China Sea. Paleoceanography 25(4):PA4205. doi:10.1029/2009pa001891

Kuroyanagi A, Kawahata H (2004) Vertical distribution of living planktonic foraminifera in the seas around Japan. Mar Micropaleontol 53(1–2):173–196. doi:10.1016/j.marmicro.2004.06.001

Lea DW, Boyle EA (1991) Barium in planktonic foraminifera. Geochim Cosmochim Acta 55(11):3321–3331

Lea DW, Spero HJ (1994) Assessing the reliability of paleochemical tracers: Barium uptake in the shells of planktonic foraminifera. Paleoceanography 9(3):445–452. doi:10.1029/94PA00151

Lea DW, Mashiotta TA, Spero HJ (1999) Controls on magnesium and strontium uptake in planktonic foraminifera determined by live culturing. Geochim Cosmochim Acta 63(16):2369–2379

Lea DW, Pak DK, Spero HJ (2000) Climate impact of Late Quaternary equatorial Pacific sea surface temperature variations. Science 289(5485):1719–1724. doi:10.1126/science.289.5485.1719

Lee H-J, Chao S-Y (2003) A climatological description of circulation in and around the East China Sea. Deep-Sea Res PT II 50(6–7):1065–1084. doi:10.1016/S0967-0645(03)00010-9

Lee TN, Johns WE, Liu C-T, Zhang D, Zantopp R, Yang Y (2001) Mean transport and seasonal cycle of the Kuroshio east of Taiwan with comparison to the Florida Current. J Geophys Res 106(C10):22143–22158. doi:10.1029/2000JC000535

Lewis E, Wallace DWR (1998) CO2SYS–Program Developed for CO_2 System Calculations ORNL/CDIAC-105 (Carbon Dioxide Information Analysis Center, Oak Ridge National Laboratory, U.S. Department of Energy, Oak Ridge, TN)

Lin Y-S, Wei K-Y, Lin I-T, Yu P-S, Chiang H-W, Chen C-Y, Shen C-C, Mii H-S, Chen Y-G (2006) The Holocene Pulleniatina Minimum Event revisited: Geochemical and faunal evidence from the Okinawa Trough and upper reaches of the Kuroshio current. Mar Micropaleontol 59(3–4):153–170. doi:10.1016/j.marmicro.2006.02.003

Liu Z, Wen X, Brady EC, Otto-Bliesner B, Yu G, Lu H, Cheng H, Wang Y, Zheng W, Ding Y, Edwards RL, Cheng J, Liu W, Yang H (2014) Chinese cave records and the East Asia Summer Monsoon. Quat Sci Rev 83:115–128. doi:10.1016/j.quascirev.2013.10.021

Marchitto TM (2006) Precise multielemental ratios in small foraminiferal samples determined by sector field ICP-MS. Geochem Geophys Geosyst 7(5):Q05P13. doi:10.1029/2005GC001018

McConnell MC, Thunell RC (2005) Calibration of the planktonic foraminiferal Mg/Ca paleothermometer: Sediment trap results from the Guaymas Basin, Gulf of California. Paleoceanography 20(2):PA2016. doi:10.1029/2004PA001077

Mulitza S, Boltovskoy D, Donner B, Meggers H, Paul A, Wefer G (2003) Temperature:$\delta^{18}O$ relationships of planktonic foraminifera collected from surface waters. Palaeogeogr Palaeocl 202(1–2):143–152. doi:10.1016/S0031-0182(03)00633-3

Niebler HS, Hubberten HW, Gersonde R (1999) Oxygen isotope values of planktic foraminifera: A tool for the reconstruction of surface water stratification. In: Wefer G (ed) Fischer G. Use of Proxies in Paleoceanography, Springer Berlin Heidelberg, pp 165–189. doi:10.1007/978-3-642-58646-0_6

Oba T (1990) Paleoceanographic information obtained by isotopic measurement of individual foraminiferal specimens. In: Wang P, Lao Q, He Q (eds) Proceedings of the First International Conference on Asian Marine Geology. China Ocean Press, Beijing, pp 169–180

Qian W, Lee D-K (2000) Seasonal march of Asian summer monsoon. Int J Climatol 20:1371–1386

Qu CH, Chen CZ, Yang JR, Wang LZ, Lu YL (1993) Geochemistry of dissolved and particulate elements in the major rivers of China (The Huanghe, Changjiang, and Zhunjiang rivers). Estuaries 16(3):475–487. doi:10.2307/1352595

Regenberg M, Steph S, Nürnberg D, Tiedemann R, Garbe-Schönberg D (2009) Calibrating Mg/Ca ratios of multiple planktonic foraminiferal species with $\delta^{18}O$-calcification temperatures: Paleothermometry for the upper water column. Earth Planet Sci Lett 278(3–4):324–336. doi:10.1016/j.epsl.2008.12.019

Rohling EJ (2007) Progress in paleosalinity: Overview and presentation of a new approach. Paleoceanography 22(3):PA3215. doi:10.1029/2007PA001437

Rosenthal Y, Boyle EA, Labeyrie L (1997) Last glacial maximum paleochemistry and deepwater circulation in the Southern Ocean: Evidence from foraminiferal cadmium. Paleoceanography 12(6):787–796

Russell AD, Hönisch B, Spero HJ, Lea DW (2004) Effects of seawater carbonate ion concentration and temperature on shell U, Mg, and Sr in cultured planktonic foraminifera. Geochim Cosmochim Acta 68(21):4347–4361. doi:10.1016/j.gca.2004.03.013

Schmidt GA (1999) Error analysis of paleosalinity calculations. Paleoceanography 14(3):422–429. doi:10.1029/1999PA900008

Schmidt MW, Lynch-Stieglitz J (2011) Florida Straits deglacial temperature and salinity change: Implications for tropical hydrologic cycle variability during

the Younger Dryas. Paleoceanography 26(4):PA4205. doi:10.1029/2011PA002157
Schmuker B, Schiebel R (2002) Planktic foraminifers and hydrography of the eastern and northern Caribbean Sea. Mar Micropaleontol 46(3–4):387–403. doi:10.1016/S0377-8398(02)00082-8
Sugiyama M, Matsui M, Nakayama E (1984) Direct determination of barium in sea water by inductively coupled plasma emission spectrometry. J Oceanogr 40:295–302
Sun Y, Oppo DW, Xiang R, Liu W, Gao S (2005) Last deglaciation in the Okinawa Trough: Subtropical northwest Pacific link to Northern Hemisphere and tropical climate. Paleoceanography 20(4):PA4005. doi:10.1029/2004PA001061
Thunell RC, Honjo S (1981) Calcite dissolution and the modification of planktonic foraminiferal assemblages. Mar Micropaleontol 6(2):169–182. doi:10.1016/0377-8398(81)90004-9
Ujiié Y, Ujiié H, Taira A, Nakamura T, Oguri K (2003) Spatial and temporal variability of surface water in the Kuroshio source region, Pacific Ocean, over the past 21,000 years: evidence from planktonic foraminifera. Mar Micropaleontol 49(4):335–364
Wang B (2006) The Asian Monsoon. Springer Praxis, Chichester
Wang Y, Cheng H, Edwards RL, He Y, Kong X, An Z, Wu J, Kelly MJ, Dykoski CA, Li X (2005) The Holocene Asian Monsoon: Links to solar changes and North Atlantic climate. Science 308(5723):854–857. doi:10.1126/science.1106296
Wang Y, Cheng H, Edwards RL, Kong X, Shao X, Chen S, Wu J, Jiang X, Wang X, An Z (2008) Millennial- and orbital-scale changes in the East Asian monsoon over the past 224,000 years. Nature 451(7182):1090–1093
Weldeab S, Lea DW, Schneider RR, Andersen N (2007) 155,000 years of west African monsoon and ocean thermal evolution. Science 316(5829):1303–1307. doi:10.1126/science.1140461
Xu X, Yamasaki M, Oda M, Honda MC (2005) Comparison of seasonal flux variations of planktonic foraminifera in sediment traps on both sides of the Ryukyu Islands, Japan. Mar Micropaleontol 58(1):45–55. doi:10.1016/j.marmicro.2005.09.002
Yanagi T (1994) Material transport in the Yellow/East China Seas. Bull Coast Oceanogr 31:239–256
Yancheva G, Nowaczyk NR, Mingram J, Dulski P, Schettler G, Negendank JFW, Liu J, Sigman DM, Peterson LC, Haug GH (2007) Influence of the intertropical convergence zone on the East Asian monsoon. Nature 445(7123):74–77
Ye F, Deng W, Xie L, Wei G, Jia G (2014) Surface water $\delta^{18}O$ in the marginal China seas and its hydrological implications. Est Coast Shelf Sci 147:25–31. doi:10.1016/j.ecss.2014.05.033
Zhang J, Letolle R, Martin JM, Jusserand C, Mouchel JM (1990) Stable oxygen isotope distribution in the Huanghe (Yellow River) and the Changjiang (Yangtze River) estuarine systems. Cont Shelf Res 10(4):369–384. doi:10.1016/0278-4343(90)90057-S
Zhang L, Liu Z, Zhang J, Hong GH, Park Y, Zhang HF (2007) Reevaluation of mixing among multiple water masses in the shelf: An example from the East China Sea. Cont Shelf Res 27(15):1969–1979. doi:10.1016/j.csr.2007.04.002
Zhang W-Z, Chai F, Hong H-S, Xue H (2014) Volume transport through the Taiwan Strait and the effect of synoptic events. Cont Shelf Res. doi:10.1016/j.csr.2014.07.010
Zweng MM, Reagan JR, Antonov JI, Locarnini RA, Mishonov AV, Boyer TP, Garcia HE, Baranova OK, Johnson DR, Seidov D, Biddle MM (2013) World Ocean Atlas 2013, Volume 2: Salinity. NOAA Atlas NESDIS 74. Silver Spring, MD